Leopold Michael Christopher Kies

Characterization of Circulation patterns in the Gulf of Cadiz based on satellite altimetry

UNIVERSIDADE DO ALGARVE

FACULDADE DE CIÊNCIAS E TECNOLOGIA

2022

Leopold Michael Christopher Kies

Characterization of Circulation patterns in the Gulf of Cadiz based on satellite altimetry

Master in Marine and Coastal Sciences

Work performed under the supervision of:

Erwan Garel

Paulo Relvas

UNIVERSIDADE DO ALGARVE

FACULDADE DE CIÊNCIAS E TECNOLOGIA

2022

Characterization of Circulation patterns in the Gulf of Cadiz based on satellite altimetry

Declaration of authorship of the work

I declare to be the author of this work, which is unique and unprecedented. Authors and works consulted are properly cited in the text and are included in the listing of references.

Leopold Kies

Faro, 30.09.2022

Copyright

Resumo

Os dados de altimetria de satélite (1993-2020) são utilizados para analisar as correntes geostróficas e a Topografia Dinâmica Absoluta (ADT) do Golfo de Cádis (GoC). O estudo do ADT anual mostrou que a subida do nível do mar do GoC está bem dentro da tendência global. A análise sazonal do ADT e dos fluxos geostróficos mostrou um padrão bilateral. Nos meses de Verão, ocorrem fortes correntes equatoriais sobre a área da plataforma, enquanto que as correntes no interior do GoC são mais fracas. No Inverno, contudo, as correntes do Equador sobre a área da prateleira são mais fracas e mais fortes no interior do GoC. Dois mecanismos em particular poderiam ser identificados para estes padrões opostos: (1) a ocorrência de ventos fortes a norte, que formam frentes de afloramento sobre a plataforma no Verão, e (2) a Corrente dos Açores que atinge e influencia os fluxos no interior do GoC no Inverno.

Além disso, são explorados os efeitos das variações do nível da água nos padrões de circulação na plataforma norte do GoC. O ADT e as circulações são comparados com medições in situ utilizando medidores de marés e Perfis Acústicos de Corrente Doppler (ADCP), respectivamente. Foi demonstrado que o ADT tem correlações moderadas a boas com as medições de marés. Não foi possível encontrar correspondência clara entre a direcção do fluxo alongshore e o declive alongshore. Isto pode ser devido ao erro do ADT perto da costa.

Além disso, os dados do Radar de Alta Frequência (HFR) são utilizados para examinar a relação entre o ADT e a Corrente Contadora Costeira (CCC) estabelecida durante cinco exemplos com as mais fortes variações do ADT. Demonstra-se que o ADT era adequado para identificar gradientes de pressão alongshore desequilibrados, que são condutores plausíveis do CCC para os exemplos analisados. As medições do HFR revelaram que os fluxos de fluxo em direcção aos pólos atingem a sua velocidade máxima dois dias após a inclinação alongshore se tornar desequilibrada.

Abstract

Satellite altimetry data (1993-2020) is used to analyze the geostrophic currents and Absolute Dynamic Topography (ADT) of the Gulf of Cadiz (GoC). The study of the annual ADT showed that the sea level rise of the GoC is well within the global trend. The seasonal analysis of ADT and geostrophic flows showed a bilateral pattern. In the summer months, strong equatorward currents occur over the shelf area, whereas the currents in the interior of the GoC are weaker. In winter, however the equatorward currents over the shelf area are weaker and stronger at the interior of the GoC. Two mechanisms in particular could be identified for these countervailing patterns: (1) the occurrence of strong northerly winds, which form upwelling fronts over the shelf in summer, and (2) the Azores Current which reaches and influences the flows in the interior of the GoC in winter.

Further, the effects of water level variations on circulation patterns at the northern shelf of the GoC are explored. The ADT and circulations are compared with in situ measurements using tidal gauges and Acoustic Doppler Current Profiles (ADCP), respectively. It was shown that the ADT has moderate to good correlations to tidal gauge measurements. No clear correspondence between the alongshore flow direction and alongshore slope could be found. This might be due to the ADT error near the coast.

Moreover, High Frequency Radar (HFR) data is used to examine the relation between ADT and Coastal Counter Current (CCC) set up during five examples with strongest ADT variations. It is shown that the ADT was suitable to identify unbalanced alongshore pressure gradients, which are plausible drivers of the CCC for the analyzed examples. The HFR measurements revealed that poleward flows reach their maximum velocity two days after the alongshore slope becomes unbalanced.

Table of content

List of Figures

List of Abbreviations

ADCP – Acoustic Doppler current profiler

ADT – Absolute Dynamic Topography

CM – Cape de Mazagan

CSM – Cape Saint Maria

CSV – Cape Saint Vincent

CTD – Conductivity, Temperature and Depth

GoC – Gulf of Cadiz

HFR – High-frequency radar

MDT – Mean dynamic topography

MSS – Mean Sea Surface

SG – Strait of Gibraltar

SLA – Sea Level Anomaly

SSH – Sea Surface Height

SST – Sea Surface Temperature

1. Introduction

1.1 Motivation

Ocean currents play a crucial role in the earth's climate system. They transport vast amounts of heat across the planet. Moreover, they are important for sea life through the transport of nutrients and organisms. Especially in regards of global climate change, it is necessary to understand ocean currents.

The Gulf of Cadiz (GoC) has been the subject of several oceanographic studies, which were mostly focused on the deep-water outflow from the Mediterranean Sea. Much less attention has been paid to the surface circulation of the GoC, which is influenced by a complex interaction of many factors (Garcia-Lafuente and Ruiz, 2007). This is especially due to the geographical location of the GoC, between the North Atlantic and the Mediterranean Sea.

The circulation patterns of the GoC are controversially debated. In particular, at the southern part of the GoC, very limited oceanographic surveys have been carried out (Machin et al., 2006). In addition, the circulation patterns of the northern part the GoC are not fully understood. The studies of large-scale circulation patterns are mostly based on Sea Surface Temperature (SST) data (Folkard et al., 1997; Relvas and Barton, 2002; Vargas et al., 2003). However, altimetry data over the ocean have been used for a long time to study the geostrophic circulation. Nowadays, recent developments in remote sensing and the growing number of satellites provide long time series of high-resolution altimetry data covering large areas at high frequency. Satellite altimetry data is in general problematic near the coast. However, recent progress has been made in terms of processing and resolution, allowing this product to be applied to nearshore areas (Etcheverry et al. 2016; Lago et al., 2021; Lin et al., 2021). Moreover, this data is available for free. In this sense, satellite altimetry data is a useful and cost-effective method to study the geostrophic circulations in the GoC.

The water circulation of the northern shelf of the GoC was investigated by recent studies (De Oliveira Junior et al., 2021; De Oliveira Junior et al., 2022; Garel et al., 2016). These studies are mainly focusing on the interaction between equatorward upwelling jets and poleward flows along the coast. However, more research is needed to identify the main driving factors, which establish poleward flows that are known as Costal Counter Current (CCC). The most plausible, supported by data in the literature, is that poleward flows are mainly driven by changes in the water level slope along the coast (De Oliveira Junior et al., 2021; De Oliveira Junior et al., 2022; Garel et al., 2016; Relvas and Barton, 2002, 2005; Sanchez et al., 2006).

High resolution satellite altimetry data provide the opportunity to explore the potential control of water level slopes on coastal circulation.

1.2 Objectives and structure

This Master thesis is divided into two parts. In the first part the Absolute Dynamic Topography (ADT) and geostrophic circulation patterns in the entire GoC are characterized. In the second part the potential effects of water level variations on circulation patterns at the northern shelf of the Gulf of Cadiz are explored.

Characterization of the ADT and geostrophic circulations patterns in the entire Gulf of Cadiz

- Determination of the ADT and geostrophic circulation patterns in the entire Gulf of Cadiz (based on a yearly and seasonal scale)
- Evaluation of the potential effect (thermal expansion) of SST on ADT

Exploration of potential effects of water level variations on circulation patterns at the northern shelf of the Gulf of Cadiz

- Determination of the concordance of ADT and geostrophic flow with in-situ measurements (tidal gauge stations, ADCPs)
- Assess potential control of ADT variations along the coast on the costal circulation (by comparison of the ADT alongshore slope with HFR circulation data)

2. Background information

2.1 Geographical frame

The GoC is a basin, which connects the North Atlantic Ocean to the Mediterranean Sea. In the north, the GoC is limited by the Iberian Peninsula. To the east, the boundary represents the Strait of Gibraltar (SG) and to the south the Moroccan coast. In this thesis the Cape de Mazagan (CM) (Figure 1) sets the southernmost boundary of the GoC. In the west, the natural border is constituted by the open ocean (i.e., between CSV and CM) (Figure 1). In scientific publications often the 9º W meridian, which is approximately crossing Cape Saint Vincent (CSV) is taken as the western boundary (Lafuente and Ruiz, 2007; Vargas et al., 2003).

In this thesis, an area will be considered that goes beyond the typical boundaries of the GoC. The zonal extent of the study area ranges from 33º N to 38º N and the meridional from 6º W to 11º W (Figure 1).

The northern continental shelf of the GoC extends from CSV to the SG. It can be divided into two sections with different morphology. The western part, from CSV to the Cape Saint Maria (CSM) and the eastern part, from CSM to the SG. At the western part, the continental shelf is narrow, typically 15 km wide with a steep slope. The eastern continental shelf is about 3 times wider and has a gentler slope. The southern continental shelf from the SG to the CM is narrow, similar to the north-western shelf, with a gentle slope (Figure 1).

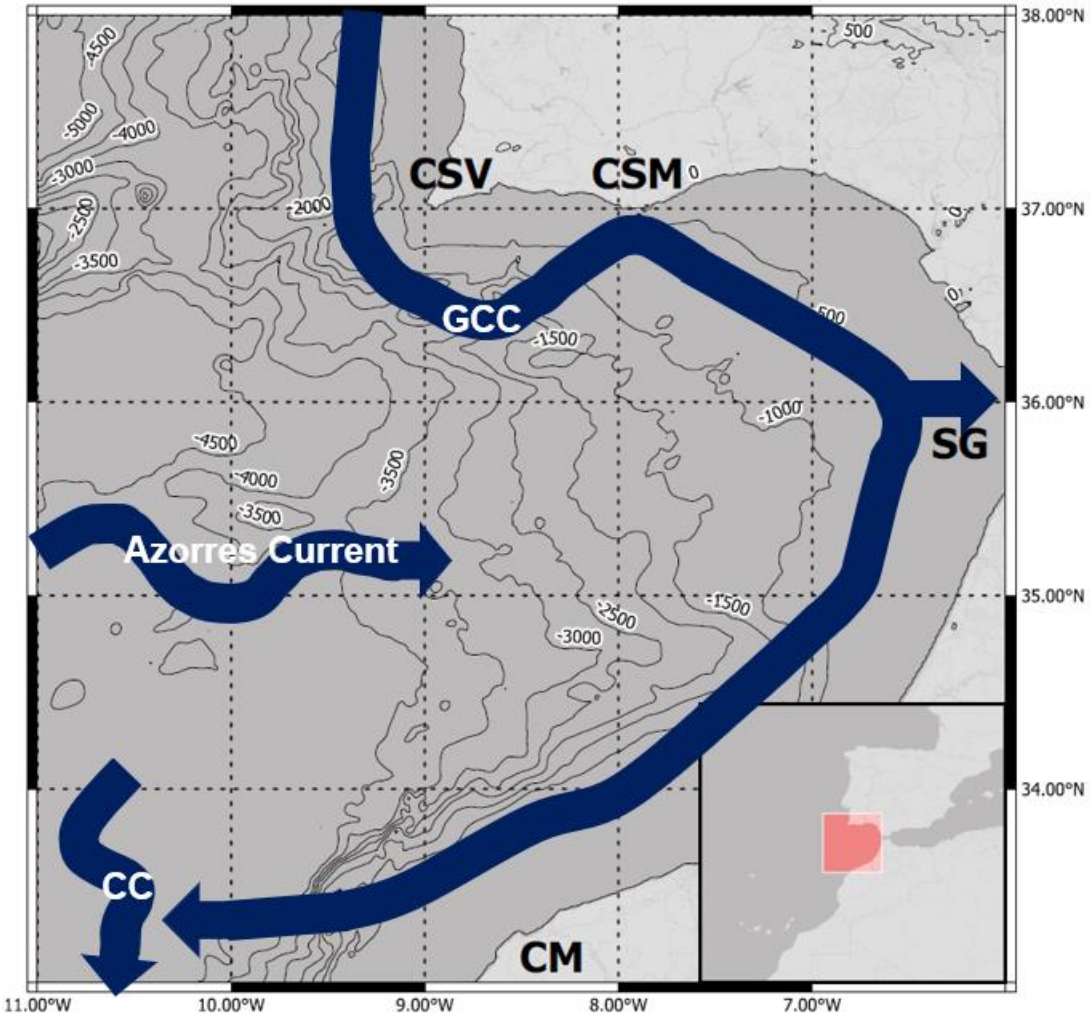

Figure 1. Study area. Blue arrows indicate the main circulation patterns: Azores Current, GCC: Gulf of Cadiz Current, CC: Canary Current. CSV: Cape Saint Vincent, CSM: Cape Saint Maria, SG: Strait of Gibraltar, CM: Cape de Mazagan.

2.2. Definition of geostrophic current

The surface geostrophic velocity is proportional to the slope of the ocean surface topography. This allows indirectly to observe geostrophic circulation through the measurement of the ocean's topography by satellites.

The ocean can be considered as geostrophic balanced in an approximation. This means that the horizontal pressure gradient is equal to the Coriolis force under certain simplifications. These simplifications include the following assumptions:

- the flow has no acceleration
- only the horizontal velocity is considered

- the only external force is gravity
- friction is negligible

Due to these simplifications, only two terms of the momentum equation remain relevant: the pressure gradient and the Coriolis force. The geostrophic approximation leads to a simple relation between surface slope and surface current.

When the geostrophic balance is established, the flow is parallel to the isobars. In the northern hemisphere, the high pressures are to the right of the flow and in the southern hemisphere to the left of the flow (Figure 2). This is caused by the opposite direction of the Coriolis force in the northern and southern hemispheres.

Furthermore, sea level variations can also cause non-geostrophic flows. This is the case if one of the previously mentioned assumptions does not apply. Friction cannot be neglected in shallow water, hence, shelf circulations are often non-geostrophic.

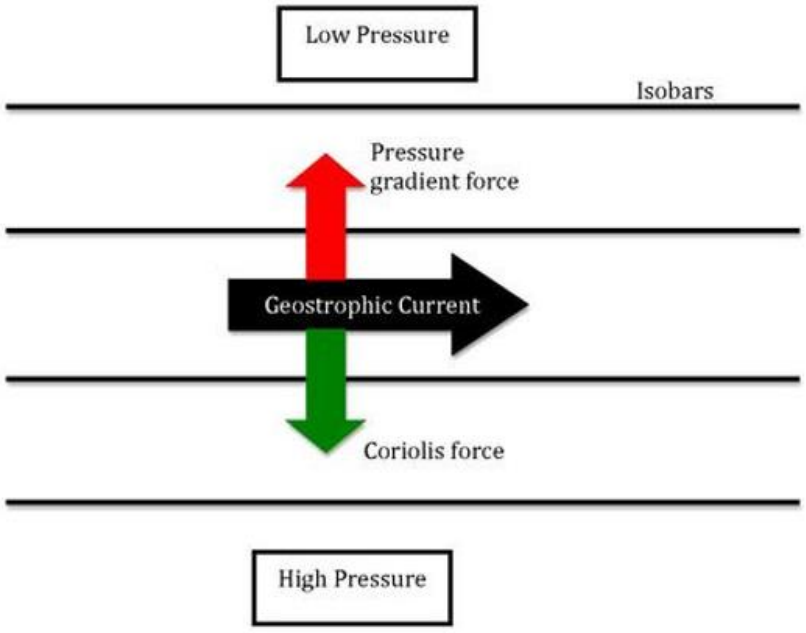

Figure 2. Established geostrophic balance. The Pressure gradient force and Coriolis force act with the same amount in the opposite direction. This causes a parallel flow along the isobars. Illustration represents the northern hemisphere (Schwart, 2010).

2.3. Circulation patterns in the Gulf of Cadiz

The general circulation patterns in the GoC are influenced by many different factors, making it a complex system due to its geographical setting. In scientific publications the circulation patterns of the GoC are controversially debated (Criado Aldeanueva et al., 2006; De Oliveira Junior et al., 2021; De Oliveira Junior et al., 2022; Folkard et al., 1997; Garel at al., 2016; Jia, 1999; Lafuente and Ruiz, 2007; Machin et al., 2006; Peliz et al., 2013; barton and Barton, 2005; Sánchez and Relvas, 2003).

On the western border, the GoC is in direct connection with the North Atlantic Ocean and is thereby influenced by oceanic processes (Carracedoa et al., 2014; Mason et al., 2011; Vargas et al., 2003). In particular, the GoC is influenced by the Azores Current and the Gulf of Cadiz Current (GCC) (Figure 1) (Johnson and Stevens, 1999; Klein and Siedler, 1989). The Azores Current meanders eastward from the Azores into the GoC. Its water transport varies seasonally, being at its minimum in spring and at its maximum in autumn (Carracedoa et al. 2014). The GCC is mainly fed by the north Atlantic gyre and flows from the north into the study area (Perez et al., 2001). The circulation patterns of the GoC have been studied through various approaches. The large-scale offshore surface circulation of the GoC is mainly assessed by SST satellite imagery (Folkard et al., 1997; Vargas et al., 2003) and by Conductivity, Temperature and Depth (CTD) measurements (Criado-Aldeanueva et al., 2006; Machin et al., 2006). Parallel to the west coast of the Iberian Peninsula the offshore equatorward GCC current proceeds (Figure 1 and 3). The GCC is strengthened by upwelling events, which occur at the west coast of the Iberian Peninsula due to strong northerly winds. These are related to large-scale wind patterns (Relvas and Barton, 2002). At the CSV the equatorward GCC flows eastward to the CSM (De Oliveira Junior et al., 2022) (Figure 3). From CSM the GCC flows south eastward to the SG. The GCC partly feeds the surface water which flows into the Mediterranean Sea through the SG (Figure 1) (Lafuente and Ruiz, 2007). Studies have mostly focused on the deep-water outflow from the Mediterranean Sea into the GoC. Fewer studies have investigated the hydrodynamic effects of the surface water flow through the SG (Folkard et al., 1997; Jia, 2000; Kida, 2006; Peliz et al., 2009; Peliz et al., 2013; Soto-Navarro et al., 2010). In general, an overturning circulation can be observed at the SG. The less dense Atlantic water flows near the surface into the Mediterranean Sea, while at the same time the denser Mediterranean water flows near the bottom into the GoC (Ambar et al., 2000). The remaining part of the GCC which doesn't flow into the SG recirculates anticyclonic along the Moroccan coast south westward to merge with the Canary current (Figure 1) (Criado-Aldeanueva et al.,2006; Machin et al., 2006). The Canary Current is the south-western part of the north Atlantic gyre which flows southward to the Canary

Islands (Figure 1). Overall, this produces an anticyclonic circulation in the GoC (Criado-Aldeanueva et al. 2006, 2009; De Oliveira Junior et al., 2022; Lafuente and Ruiz, 2007; Vargas et al. 2003). It is assumed that the general circulation in the GoC is anticyclonic during summer and alternates temporarily with a less clear but cyclonic circulation in winter (Lafuente and Ruiz, 2007).

More recently, studies have been focusing on the circulations of the northern shelf of the GoC. The self circulations have been investigated with ADCP measurements and High-Frequency Radar data (De Oliveira Junior et al., 2021; De Oliveira Junior et al., 2022; Garel et al., 2016). The northern shelf of the GoC consists of two smaller shelf circulations. At CSM the GCC partly recirculates over the shelf. Near the coast, the flow is alongshore and balanced between the equatorward and poleward (CCC) directions (Figure 3) (De Oliveira Junior et al., 2022). Investigations with ADCP and HFR data assume that CCC develop during relaxation of northerly winds which results in an unbalance alongshore pressure gradient (De Oliveira Junior et al., 2021; De Oliveira Junior et al., 2022; Garel et al., 2016). De Oliveira Junior et al. (2022) showed that the shelf flows are less prominent at the eastern bight than in the western bight of the northern GoC (Figure 3).

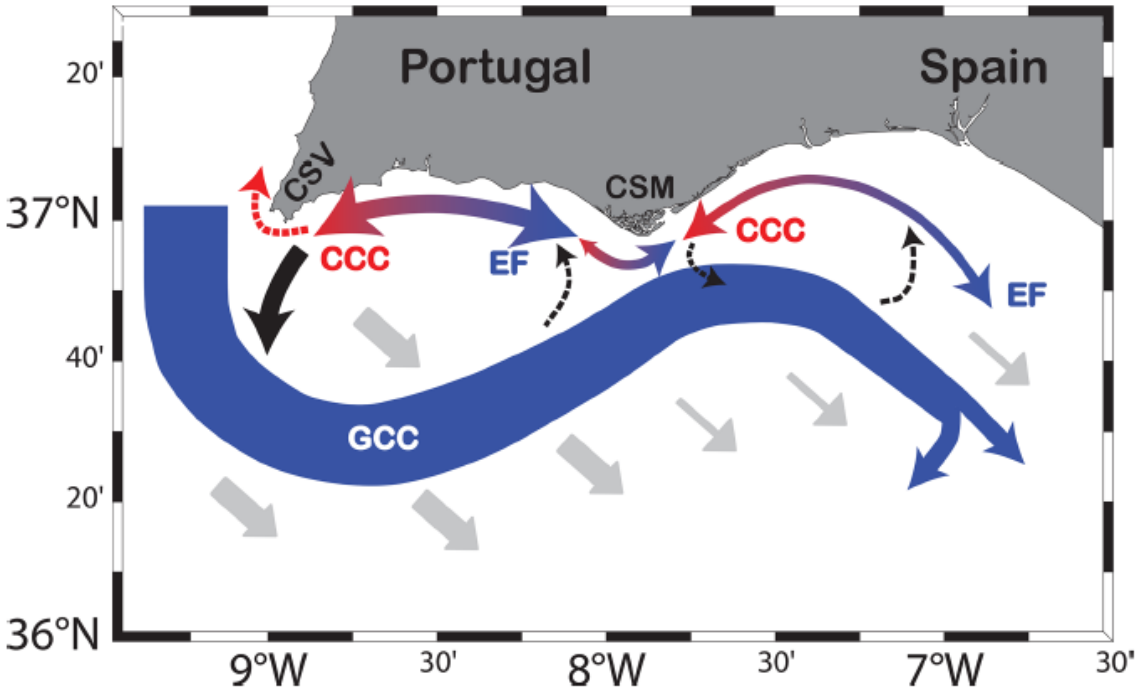

Figure 3. Circulation pattern of the northern part of the GoC (De Oliveira Junior et al., 2022). Red (blue) arrows indicate the direction of warm (cold) water advection. Dashed arrows indicate a sporadic circulation. The flow magnitude is schematically represented by the size of the arrows. GCC: Golf of Cadiz Current; CCC: Costal Counter Current (poleward current); EF: Equatorward Current.

3. Data

In this thesis, multiple data sets are used. These are obtained by various devices like satellites, ADCPs, tidal gauge stations and HFR antennas. In this chapter data acquisition and data processing are explained.

3.1 Satellite data

Two gridded reanalysis satellite datasets are used. The first one provides ADT and the u- and v-components of the geostrophic current. The second one provides SST. These datasets are optimally interpolated L4 reprocessed products provided by Marine Copernicus (www.marine.copernicus.eu). So-called "L4" means that the data of all missions are combined into one file (Copernicus, 2022).

The ADT and the geostrophic current u- and v-components are obtained from the dataset SEALEVEL_EUR_PHY_L4_MY_008_068 (Copernicus, 2022). The product is processed by DUCAS (Data Unification and Altimeter Combination System). It combines satellite altimetry data of the missions: Jason-3, Sentinel-3A, HY-2A, Saral/AltiKa, Cryosat-2, Jason-2, Jason-1, T/P, ENVISAT, GFO, ERS1/2. The spatial resolution is 0,125° x 0,125° which corresponds approximately to a resolution of 14 km x 11 km in the GoC and the temporal resolution is one day. The satellite data over the period 01 Jan 1993 - 31 Dec 2020 with the spatial extension of 38° N to 33° N and 6° W to 11° W will be used. The nearest valid data points to the coast varies with the location between approximately 1,5 km and 15,5 km.

$$ADT = SLA + MDT \qquad (1)$$

The ADT is calculated according to equation 1. The Sea Level Anomaly (SLA) is computed as the difference between the measured Sea Surface Height (SSH) and the Mean Sea Surface (MSS) MSS_CNES_CLS15 which is the 20 years mean between 1993 and 2012. The Mean Dynamic Topography (MDT) MDT_CNES_CLS_2018 from Mulet et al. (2021) is used. The MDT is referenced to the 20 years mean between 1993-2012 above the geoid GOCO 05s. The ADT thus reflects the difference between the instantaneous height of the sea level and the reference geoid (Figure 4).

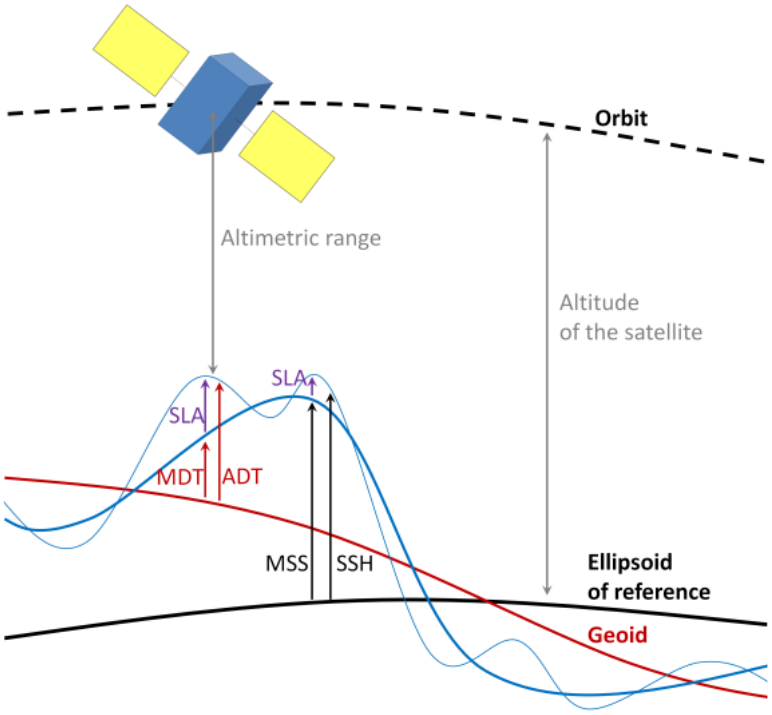

Figure 4. Overview of the different references of satellite altimetry (Autret et al., 2022). ADT: Absolute Dynamic Topography, MDT: Mean Dynamic Topography, SLA: Sea Level Anomaly, MSS: Mean Sea Surface, SSH: Sea Surface Height.

$$u = -\frac{g}{f} * \frac{\partial ADT}{\partial y} \qquad (2)$$

$$v = \frac{g}{f} * \frac{\partial ADT}{\partial x} \qquad (3)$$

To calculate the geostrophic current, the ADT instead of the SSH is used in this thesis. As the ADT refers to the reference geoid, it represents the absolute potential energy of a water parcel. The SSH do not refer to the reference geoid, thus the absolute potential energy is not determined. With the ADT it is possible to calculate the geostrophic current by applying equations 2 and 3. However, the computed velocities are extracted from Copernicus (Copernicus, 2022). The u-component is the zonal geostrophic velocity (positive eastward) and v-component is the meridional geostrophic velocity (positive northward). The equation includes: *f* [rad/s] as the Coriolis parameter, *g* [m/s^2] as the acceleration of gravity, *dx, dy are*

the distance between two consecutive grid nodes in the zonal and meridional directions and *ADT* as the Absolute Dynamic Topography.

To correctly classify the research results, it is necessary to estimate the error of the ADT. Considering the construction of the ADT, the error is composed of the errors of SLA and MDT. In principle, the SLA is underestimated due to the origin of construction. The average results of different missions are used to calculate the SLA (Copernicus, 2022). The SLA error is provided in the product SEALEVEL_EUR_PHY_L4_MY_008_068 for every grid point. The SLA error is generally larger near the coast (up to 2.5 cm) than in the interior of the GoC (up to 1 cm) (Annex: SLA error). The MDT error is dominated by oceanic variability patterns (Mulet et al., 2021; Rio et al.,2011). According to Rio et al. (2011), an MDT error of approximately 2 cm can be considered in the GoC. By the consideration of the errors of SLA and MDT a maximum error of approximately 4.5 cm over the shelf and approximately 3 cm at the interior of the GOC is assumed.

Further, SST data is used which is reprocessed by Ifremer (Institut Français de Recherche pour l'Exploitation de la Mer) to produce gap-free time series. The gridded reanalysis data SST_ATL_SST_L4_REP_OBSERVATIONS_010_026 is used from 01 Jan 1993 to 31 Dec 2020. The dataset has a spatial resolution of 0,05° x 0,05° which corresponds approximately to 5,5 km x 4,5 km. The product represents the daily mean temperature at the depth of 20 cm from the sea surface (Autret et al. 2021).

3.2 Velocity data (ADCP, HFR)

The datasets of three ADCP's are used which are provided by CIMA (Centro de Investigação Marinha e Ambiental da Universidade do *Algarve)*. All ADCP devices are located at the northern shelf of the GoC, one in the western bight (ADCP Quarteira) and two at the eastern bight (ADCP Cacela and Armona) (Figure 5). The ADCP station Cacela (37º 6.45´N 7º 29.79'W, 23 water depth) includes measurements between the period Jul 2019 to Oct 2019. At the Armona station (37º 0.65'N 7º 44.48'W, 23 m water depth) data from Dec 2017 to Oct 2020 will be used. The ADCP station Quarteira (37° 03.45'N 8° 06.62'W, in 9 m water depth) provides data from Jul 2014 to Dec 2020. The ADCP dataset includes daily average u- and v- velocities along the water column. Further, the ADCP data are low pass filtered to remove tides and other high frequency oscillations.

Along the south coast of Portugal and Spain, four HFR antennas are available. They are located in Sagres, Alfazina, Vila Real de Santo Antonio and Mazagon (Figure 5). Each antenna sends radar waves out at 13.5 MHz, which are reflected by the ocean surface (De Oliveira Junior et al., 2022). Due to the velocity of the ocean surface the frequency of the

backscattered radar wave is Doppler shifted. By overlapping the radar signals from at least two stations, it is possible to compute the surface flow (speed and direction). The HFR data from Feb 2016 to Oct 2020 will be used, which has the largest coverage of the shelf of the GoC (since during this period all four antennas were operating). The system provides surface velocities with spatial resolution of 1,5 km up to 60 km from the coast and the temporal resolution is hourly (CMEMS, 2017).

3.3 Tidal gauge data

Tidal gauge water level measurements are taken to validate the satellite altimetry data. For this purpose, the monthly averaged tidal gauge datasets of two stations are used. The tidal gauge station Huelva (37º 7.80´N 6º 49.80'W) (Figure 5) consists of sea level measurements from Oct 1996 to Dec 2020. The station Bonanza (36° 48.00'N 6° 20.40'W) (Figure 5) provides sea level data from Jul 1992 to Dec 2020. The tidal gauge data is obtained from MITMA (Ministerio de Transportes, Movilidad y Agenda Urbana) and downloaded from www.puertos.es.

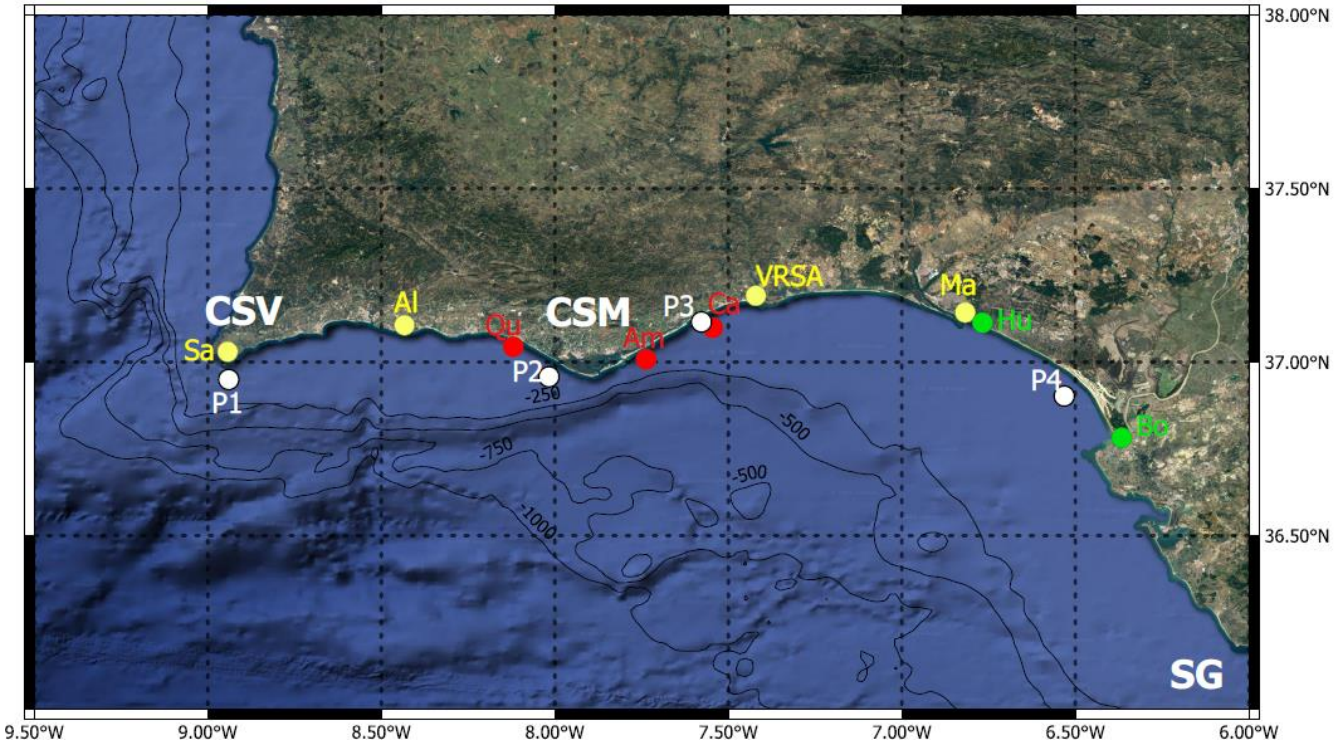

Figure 5. Northern shelf of the GoC. Location of HFR antennas (yellow points, with Sa: Sagres; AL: Alfanzia; VRSA: Vila Real de Santo António; Ma: Mazagon), ADCP mooring (red points, with Qu: Quarteira; Am: Armona; Ca: Cacela), Tidal guge stations (green points

4. Methodology

4.1 Characterization of the ADT and geostrophic circulations

4.1.1 ADT and geostrophic circulation patterns in the entire Gulf of Cadiz

To characterize the ADT and geostrophic circulation patterns the time-series are reprocessed. The average signals of the ADT and geostrophic current (1993-2020) are computed. Further, the linear trend is calculated from the annual average ADT and geostrophic current. The average ADT and geostrophic current is calculated for each of the seasons: Winter (Dec-Feb), Spring (Mar-May), Summer (Jun-Aug) and Autumn (Sep-Oct). Moreover, the seasonal anomaly of the ADT and geostrophic circulations are calculated. This is done by removing the 28 years average from each seasonal map. These maps clearly show how the individual seasons differ from the average.

4.1.2 Potential effect (thermal expansion) of SST on ADT

It is assessed if the SST influences the ADT. The objective is to clarify the potential effect of thermal expansion on the ADT. The Spearman's coefficient is calculated to determine the concordance of the two time-series. For this purpose, the SST resolution (0.05° x 0.05°) is interpolated to fit the ADT resolution (0.125° x 0.125°).

4.2 Characterization of the circulation patterns at the northern shelf of the GOC

4.2.1 Concordance of ADT and geostrophic flow with in-situ measurements (tidal gauge stations, ADCPs)

To determine the concordance of the ADT and geostrophic flow they are compared with tidal gauge and ADCP data. The datasets of the two tidal gauge stations Huelva and Bonanza are taken to validate the ADT measurements near the coast. The ADT data points closest to the respective stations are chosen. The distance to the nearest ADT data point from the Huelva station is approximately 12 km and approximately 20 km from the Bonanza station. The monthly average ADT is calculated to ensure that the two-time series have the same length. The Spearman's coefficient is calculated to determine the strength of the correlation between the two time-series.

Further, the geostrophic circulations are compared with the measurements of three ADCPs. This is done to check the importance of geostrophicity as a driver of the shelf circulation. The ADCP velocity was calculated by taking the average velocity over the respective water

column, low-pass filtered to remove the tidal signal. The Spearman's coefficient is calculated for the u-component at Quarteira, Armona and Cacela stations with the respective u-component of the geostrophic flow. The ADCP Cacela is approximately 7 km away from the closest satellite record, ADCP Armona approximately 10 km and ADCP Quarteira approximately 14 km.

4.2.2 Potential control of ADT variations along the coast on the coastal circulation

The ADT slope and the (alongshore) circulation at the northern shelf are described in more detail. Special attention is devoted to the correlation between the development of westward flows (CCC) along the coast and variations in the alongshore slope, to test the hypothesis that sea level variations along the coast is the main driver of these flows (De Oliveira Junior et al., 2021; De Oliveira Junior et al., 2022; Garel et al., 2016).

The time series of four ADT points are chosen along the northern shelf of the GoC. The points P1 (36° 56.25' N 8° 56.25' W) and P2 (36° 56.25' N 8° 3.75' W) are located in the western bight of the northern GoC. P1 is approximately 6 km south of CSV and P2 approximately 10 km offshore, west of CSM (Figure 5). Whereby P3 (37° 7.75' N 7° 33.75' W) and P4 (36° 56.25' N 6° 33.75' W) are in the eastern bight. P3 is located north-west of CSM approximately 7 km offshore (Figure 5). P4 is located on the eastern side of the east bight approximately 6 km offshore (Figure 5). Four ADT alongshore slopes are calculated. In the western bight (P1-P2), around CSM (P2-P3), eastern bight (P3-P4) and over the entire northern shelf (P1-P4) (Figure 5). Positive values of the alongshore slope indicate a higher water level westward and negative values a higher water level eastward. The annual mean and the trend are calculated for the four ADT slopes.

The ADT alongshore slope is compared with the ADCP velocity measurements. The Spearman correlation of the ADCP Quarteira and the ADT slope at the western bight (P1-P2) as well as the ADCPs Cacela and Armona and at the ADT slope of the eastern bight (P3-P4) is calculated to evaluate the correspondence. Moreover, the cross correlation is calculated to detect temporal lags between the velocity and respective ADT slope.

Further, it is examined whether the HFR current data correspond to the ADT slope. In particular it examines if CCC develops when the alongshore slope becomes unbalanced (De Oliveira Junior et al., 2021; De Oliveira Junior et al., 2022; Garel et al., 2016). Therefore, the time series of the ADT slope is examined for periods of strong negative changes of the ADT differences. These abrupt changes in the ADT indicate an unbalanced slope. The daily average HFR circulations are visualized at the dates of these initially ADT slope changes.

5. Results

The Results are divided into two parts. In the first part, the results of the entire GoC are presented. The second part focuses on the results of the northern continental shelf of the GoC.

5.1 Characterization of the entire GoC

5.1.1 ADT signal

The linear trend of the ADT in the Gulf of Cadiz has an average increase of 3.15 mm/year (R^2: 0.85) at the study area for the period of 1993 – 2020 (Figure 7). Figure 6 shows the mean ADT map over the 28 years (1993 – 2020). The mean ADT distribution shows a gradual north-south increase. The ADT increases from a minimum of 6.13 cm from the north up to 18.80 cm in the south. It is noticeable that from the west coast of Portugal to the SG along the Iberian coast low ADT values are present (CSV, CSM, SG in Figure 7). This area roughly follows the northern continental shelf and slope. Further, at the SG an abrupt ADT change can be observed. Here the water level rises rapidly from north to south over a short distance. In the south of the study area, the ADT level rises again sharply. This area of high ADT level at south extends to a narrow strip along the Moroccan coast where the ADT level shows lower values (CM in Figure 7).

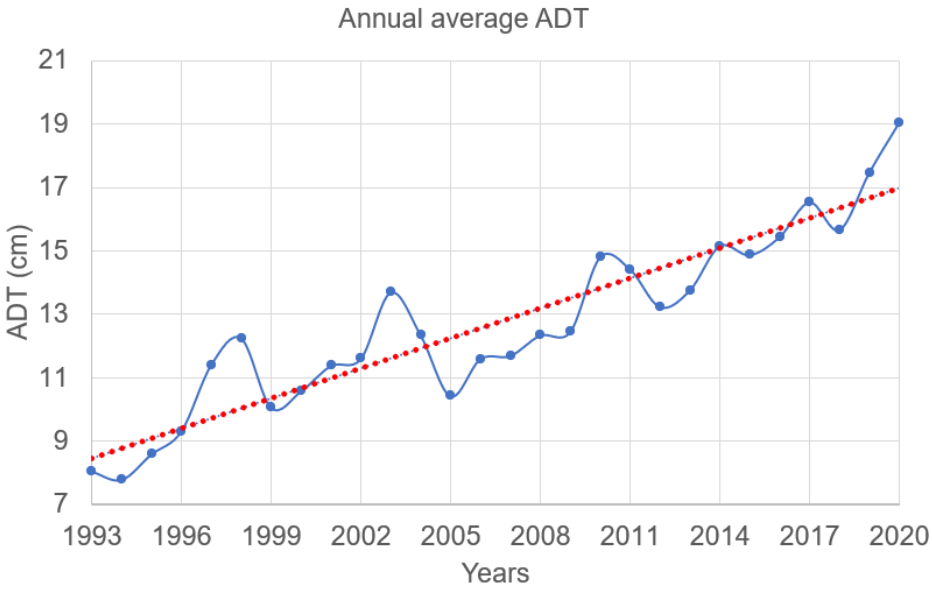

Figure 6. Annual average ADT with red trendline (1993- 2020)

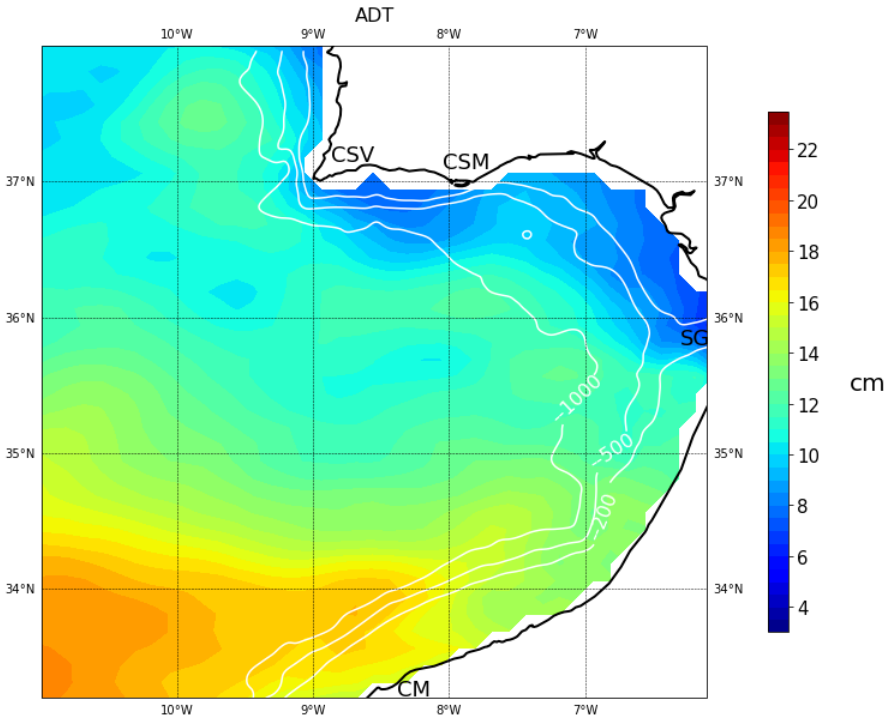

Figure 7. Average ADT (1993-2020)

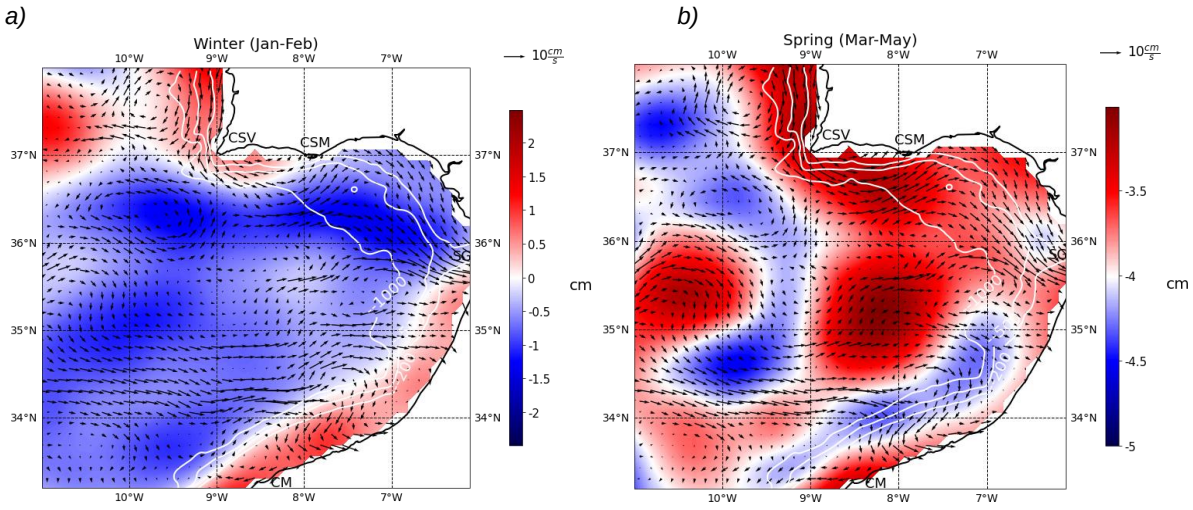

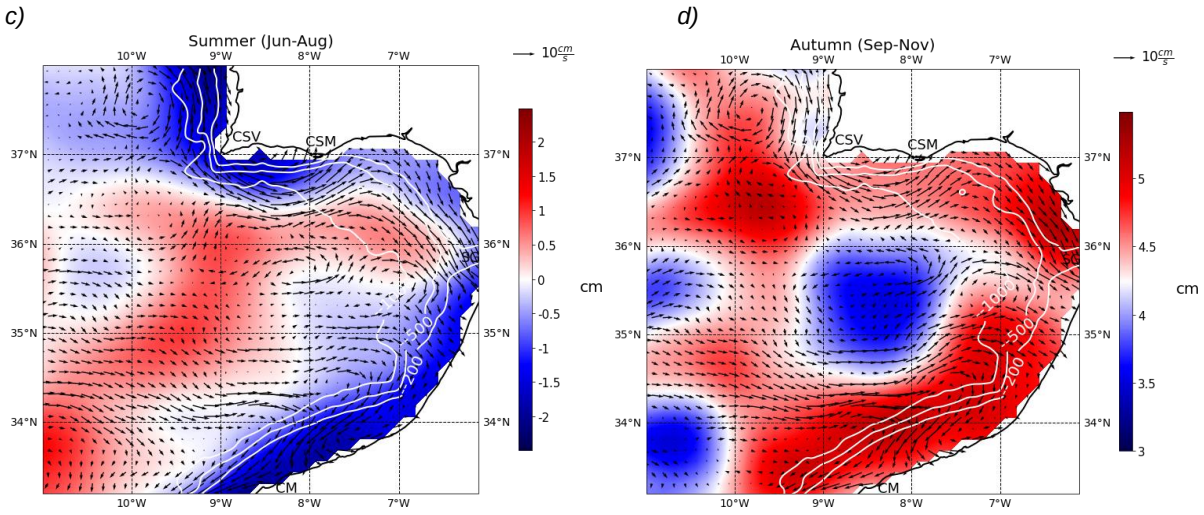

Figure 8. Seasonal ADT anomalies. a) Winter, b) Spring, c) Summer, d) Autumn. Note the different scaling in spring and autumn.

In order to detect potential seasonal patterns, the seasonal ADT anomalies are calculated. Red colors indicate positive anomalies and blue colors indicate negative anomalies.

The highest ADT values (17.16) are observed in autumn and the lowest in spring (8.88 cm). In winter and summer, the ADT values are very similar (12.31 cm, 12.55 cm). Figure 8 shows that in spring the anomaly values are negative over the whole study area whereas they are positive in autumn. In winter and summer, on the other hand, both positive and negative anomalies can be observed.

In winter, positive anomalies along the shelf at the west coast of Portugal and around CSV are present (Figure 8 a). Whereas east of CSM towards the SG negative anomaly values are observed. From the SG south-eastward along the Moroccan coast positive ADT anomaly values are present over the shelf. In the interior of the GoC are only negative ADT anomalies in winter. Spring is the season with the lowest ADT. This is illustrated in Figure 8 b) by the presence of just negative ADT values throughout the study area. Nevertheless, regional differences can be seen. Figure 8 c) shows the ADT anomalies in summer. Lower ADT anomaly values are located along the west coast of Portugal around CSV towards the SG. The lower ADT values are located over the north continental shelf of the GoC. The highest ADT anomaly values are in the south-west of the study area whereas lower ADT values are near CM. This represents a west-east gradually decrease of the ADT towards the Moroccan coast. In general, it is observed that along the coast of the Iberian Peninsula and Morocco the ADT anomaly shows negative values. Positive anomaly values, on the other hand, can be observed more inside the GoC. The highest ADT values are reached in autumn. This is

also shown by the exclusively positive ADT anomaly values over the entire study area (Figure 8 d).

5.1.2 Potential effect (thermal expansion) of SST on ADT

The ADT is compared with the SST patterns to verify the effect of thermal expansion on the ADT. The Spearman correlation is calculated between the ADT and SST time-series at every grid point (Figure 9). The Spearman correlation coefficient ranges between 0.29 (p-value < 0.05) and 0.62 (p-value < 0.05). It is observed that the interior of the GoC has a higher correlation than the coastal areas. Especially over the shelf, the Spearman correlation is lower. However, higher correlations (> 0.5) occur at the shelf in the eastern bay of the GoC (Figure 9). Figure 10 shows the ADT / SST time series near the northern shelf slope where a high spearman correlation was detected (> 0.5). The seasonal pattern of the two time series (ADT / SST) correspond well. However, the highest SST values occur mostly in August whereby the highest ADT vales are detected in October. This shows that the ADT has a lag of two months behind the SST.

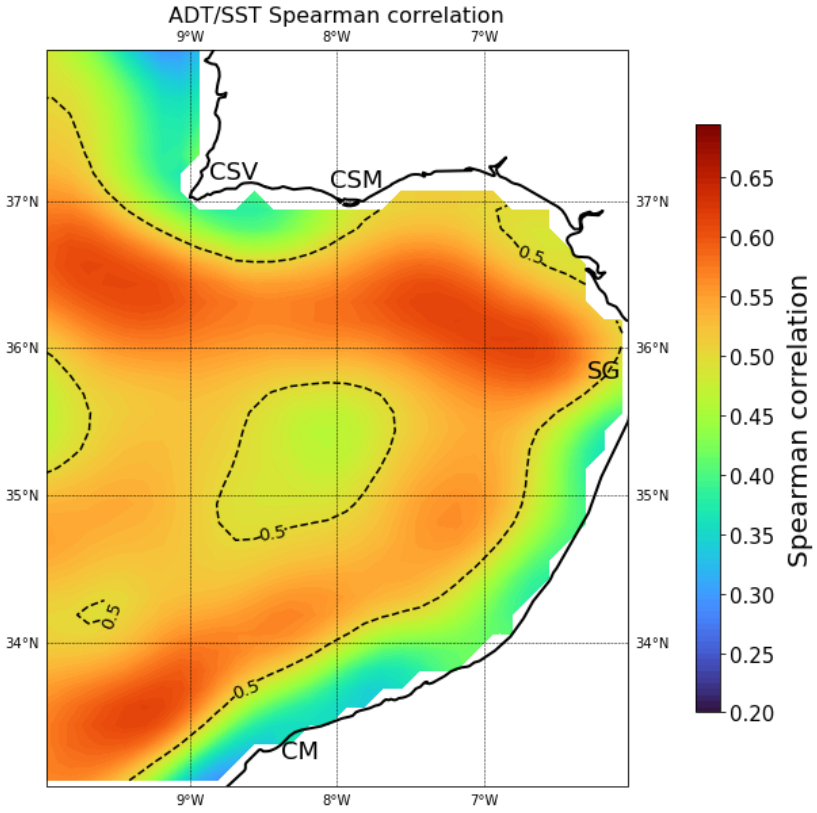

Figure 9. Spearman correlation ADT/SST

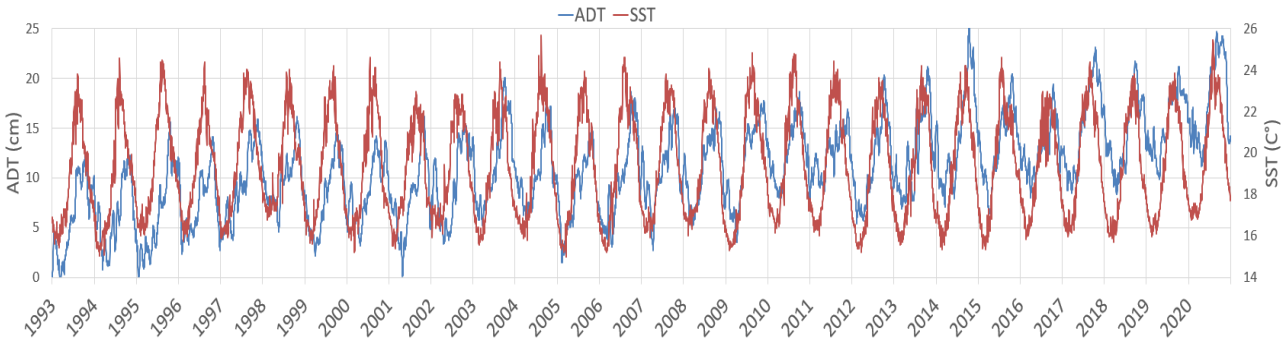

Figure 10. Comparison of ADT and SST time series.

5.1.3 Geostrophic circulation signal

The average surface geostrophic circulation pattern of the 28 years (1993 to 2020) in the GoC is calculated (Figure 11). In the study period, a linear increase of the average geostrophic velocity is observed of 0.03 cm/year (R^2: 0.38). The average geostrophic velocities vary within the study area between 0.05 cm/s up to 12.71 cm/s (Figure 11). Parallel to the west coast of Portugal a southward propagating current is present which is identified as GCC. The GGC flows equatorward and has a zonal extent of up to 125 km offshore from the west coast of Portugal. This corresponds approximately to a water depth of 1000 m. At the CSV, the current flows around the cape eastward along the north shelf to the CSM. A clear increase of the current velocity is observed around the CSV. After the current rounded the CSM, the current flows mostly over the shelf and its slope of the eastern bay towards the SG. East of CSM, the velocity is decreases at first and then again gradually increases towards the SG. The inflow into the SG reaches a speed of up to 12.70 cm/s which represents the maximum average velocity of the entire study area. Furthermore, a current is observed which is flowing from the interior of the GoC into the SG. This current occurs approximately 200 km west of the SG and propagates to the east in the SG. In the southern part of the study area, an eastward propagating current between 34° N - 35° N and 36° N is observed which is identified as a part of the Azores Current. The current flows from the Atlantic into the GoC and reaches its highest velocities between 8° W and 9° W. East of 8° W the current recirculates anticyclonically and flows along the Moroccan continental shelf in south-western direction.

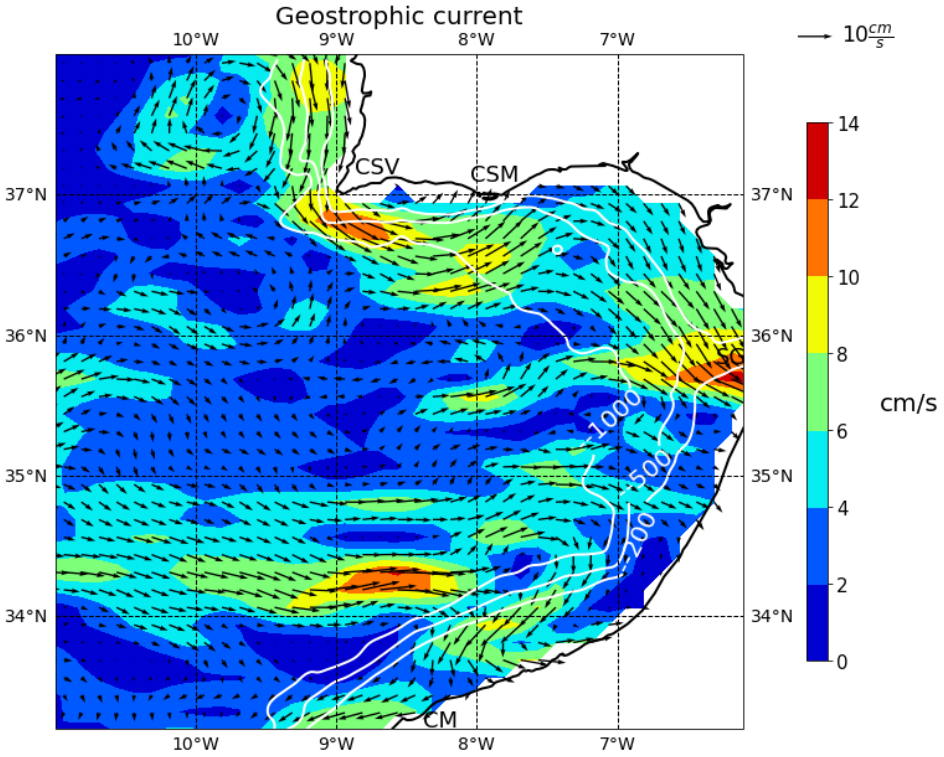

Figure 11. Average geostrophic current (1993-2020)

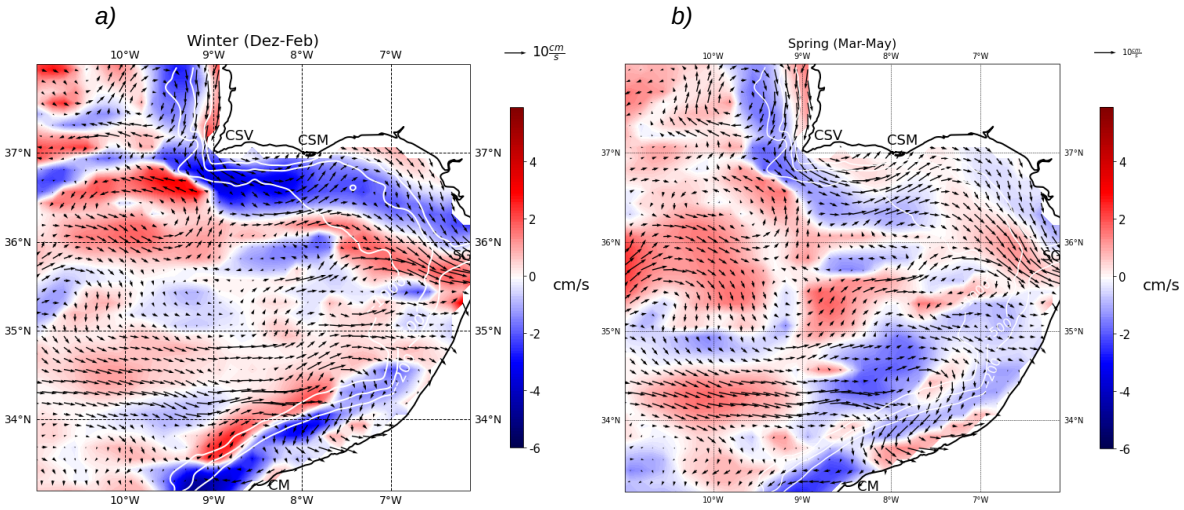

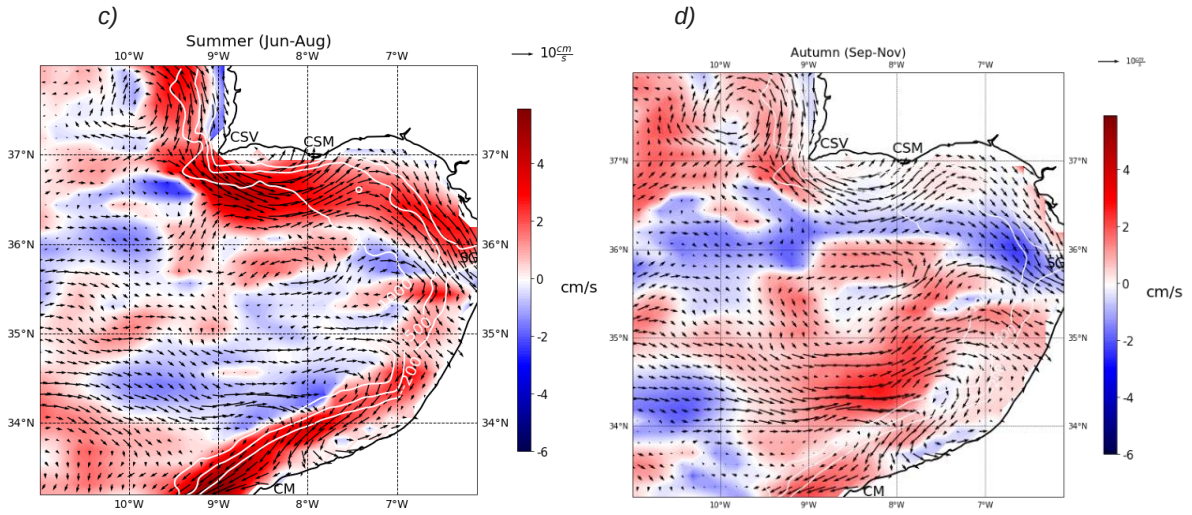

Figure 12. Seasonal surface geostrophic current patterns. For each season, the average geostrophic flows and the seasonal anomaly are shown. a), b) Winter; c), d) Summer.

Further, the seasonality of the geostrophic circulation is studied. The same seasonal classification is used as for the ADT. The seasonal average and seasonal anomaly of the geostrophic velocity is calculated.

The average surface geostrophic currents are lowest in winter (4.00 cm/s) and strongest in summer (4.70 cm/s). The seasons of spring (4.12 cm/s) and autumn (4.34 cm/s) are transitional periods between these two extremes. Through the anomaly map in winter season (Figure 12 a) it is evident that the equatorward flow over the continental shelf of the Iberian Peninsula and along the Moroccan coast is weaker. On the other hand, the geostrophic currents velocity inside the GoC are increased in winter. In particular, this is evident by the fast-flowing current (Azores Current) at the interior of the GoC between 34°N - 35°N and 36°N. This current is propagating eastward into the study area. In summer, on the other hand, a controversial pattern is observed (Figure 12 c). High flow velocities are along the coast of the Iberian Peninsula and the Moroccan cost in the summer season. The anomaly velocities over the entire continental shelf of the GoC are increased compared to winter. However, the anomaly figure in summer indicates that the eastward propagating flow between 34°N - 35°N and 36°N is weaker in the summer season. Generally, it can be said that in summer the equatorward propagating flow over the continental shelf of the GoC is pronounced. On the other hand, the currents within the GoC are weaker. The contrasting flow patterns in winter and summer leads also to two different modes at the SG. In winter the water inflow into the SG comes more from the interior of the GoC, where higher velocities are observed than from the northern continental shelf region (Figure 12 a). In summer, on the other hand, the inflowing water into the SG comes from the northern shelf of the GoC (Figure 12 c).

5.2 Characterization of the ADT and circulations along the northern shelf of the GoC

5.2.1 Concordance of ADT and geostrophic flow with in-situ measurements

The ADT is compared with in-situ measurements of two tidal gauge stations. This is done to validate the ADT records near the coast. The daily mean sea level of the tidal gauge stations Huelva (37º 7.80´N 6º 49.80'W) and Bonanza (36° 48.00'N 6° 20.40'W) (Figure 5) which are located at the coast of Spain are used. The daily mean ADT grid points closest to the respective stations is taken and compared. Figure 13 show the tidal gauge measurements with the respective ADT. The ADT signal has roughly the same pattern as the tidal gauge measurements. The Huelva measurements and the respective ADT has a Spearman's correlation coefficient of 0.52 (p-value < 0.05). The Bonanza station measurements and the respective ADT has a Spearman's correlation coefficient of 0.51 (p-value < 0.05). However, the tidal gauge measurements have a greater range of variation than the ADT measurements. The tidal gauge stations measurements have a variation range of 64 cm (Bonanza) and 43 cm (Huelva). Whereby the respective ADT measurements have a variation range of 18 cm (Bonanza) and 22 cm (Huelva). Furthermore, the trend of the annual average of the two tidal gauge stations was calculated. The tidal gauge measurements from Bonanza show a linear trend of 0.30 cm/year (R-square: 0.38). Huelva, however, shows a negative trend of -0.08 cm/year (R-square: 0.08) (Annex: Tidal gauge trend).

a)

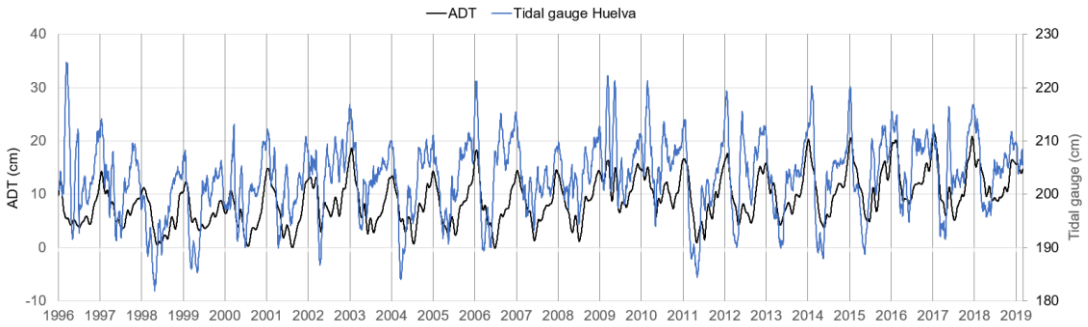

b)

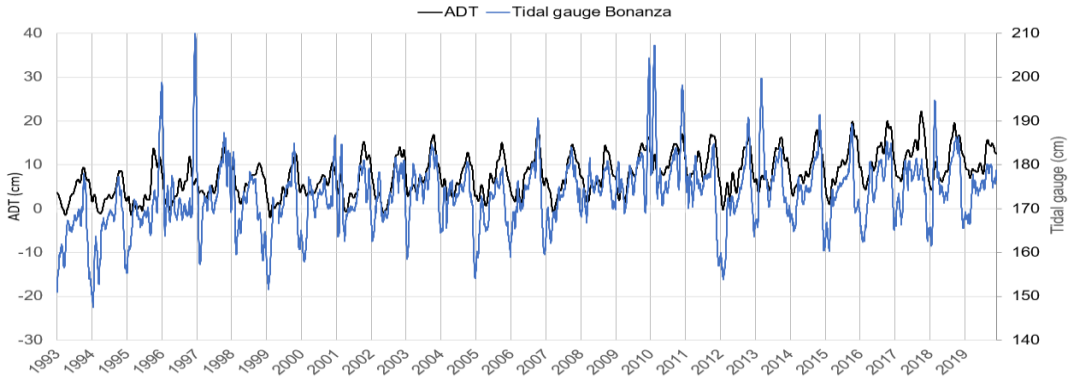

Figure 13. Comparison of ADT and Tidal gauge stations a) Huelva b) Bonanza

To evaluate the geostrophicity of the shelf circulation the geostrophic flow is compared with the available ADCP measurements. The measurements of the ADCP`s Quarteira, Armona and Cacela are compared with the respective grid point of the geostrophic flow. The current measurements of the ADCP`s Quarteira and the respective data point has a Spearman's correlation coefficient of 0.13 (p-value < 0.05) (Figure 14 a, b, c). However, this is the only correlation that was found. No significant correlation is observed between the ADCPs Armona and Cacela and the respective geostrophic flow.

a)

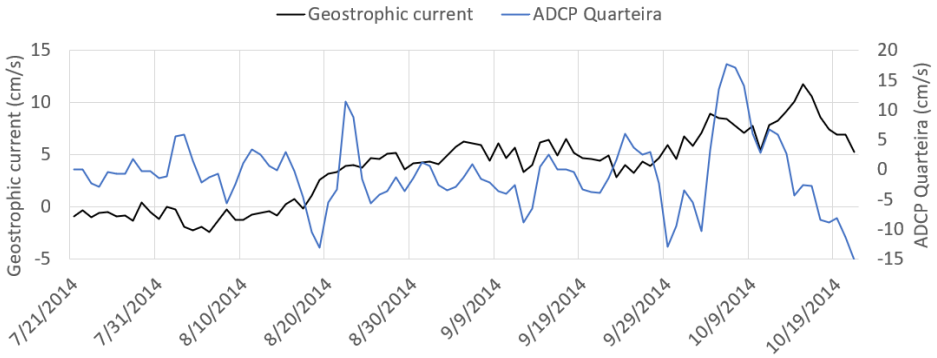

b)

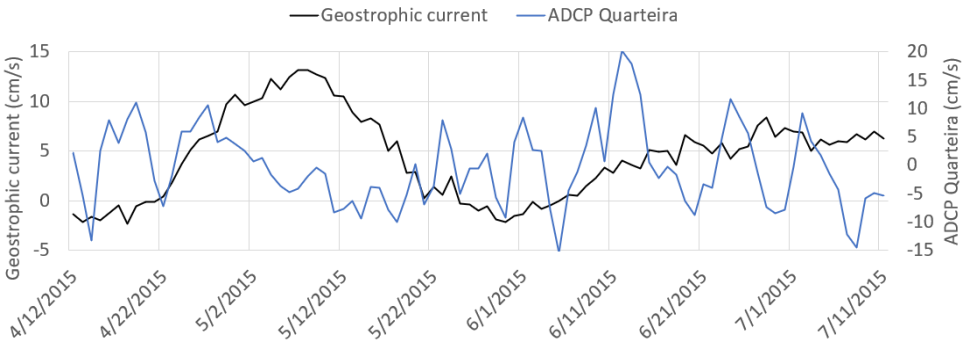

c)

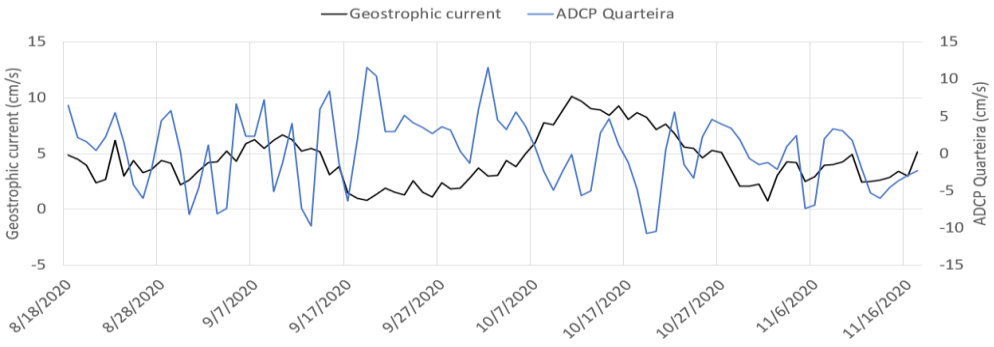

Figure 14. Comparison of ADCP Quarteira and geostrophic flow. a) 2014; b) 2015; c) 2020.

5.2.2 ADT alongshore slope at the northern shelf of the GoC

Four ADT datapoints are compared with each other to detect a possible ADT slope along the coast (Figure 5). Figure 15 a) show the ADT difference between P1 (CSV) and P2 (CSM). Between 1993 and 2010 the graph shows mostly positive values (P1 > P2) except for the years 1994, 2000 and 2008. Further it is shown that P1 is in maximum 2,11 cm higher than P2 in 1995. From 2011 to 2020 the ADT difference is predominantly negative (P1 < P2) except for the years 2013, 2017 and 2018. P1 is in maximum -0.59 cm lower than P2 in 2016. The time series has a negative trend. A yearly decrease of -0.05 cm (r-square: 0.37) of the ADT difference is observed. The monthly difference between P1 and P2 is shown in Figure 16 a). From January to June P1 has higher ADT values than P2. However, in maximum P1 is 1.44 cm higher than P2 in January. In the months July, August, and September the ADT of P1 is lower than of P2. In maximum P1 is -0.28 cm lower than P2 in August. From October to December P1 is again higher than P2.

a)

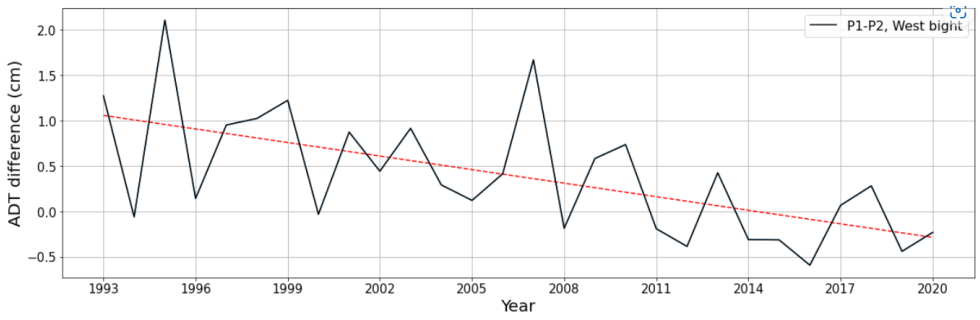

b)

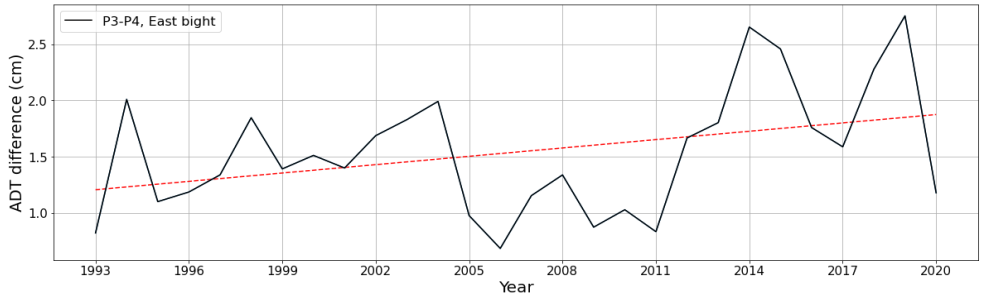

c)

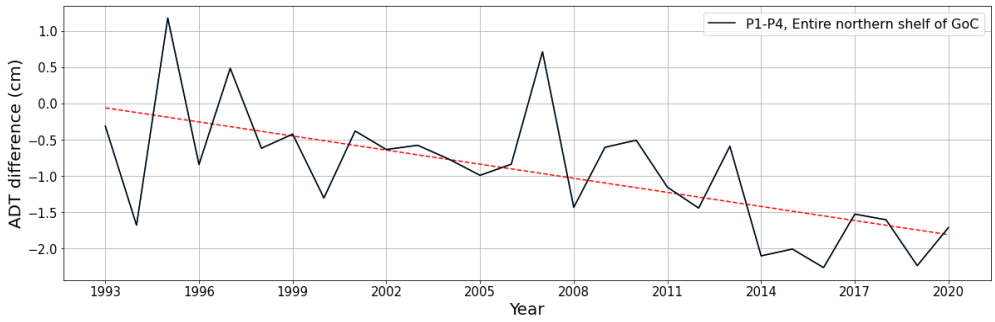

Figure 15. ADT slopes. a) West bight; b) East bight; c) Entire northern shelf of GoC

a)

b)

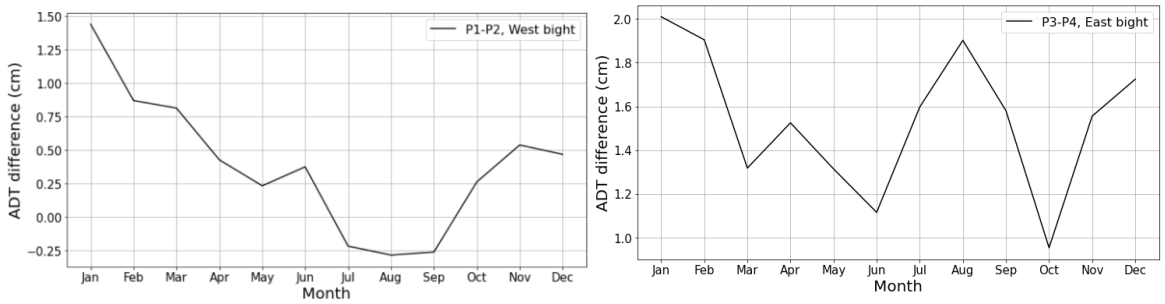

c)

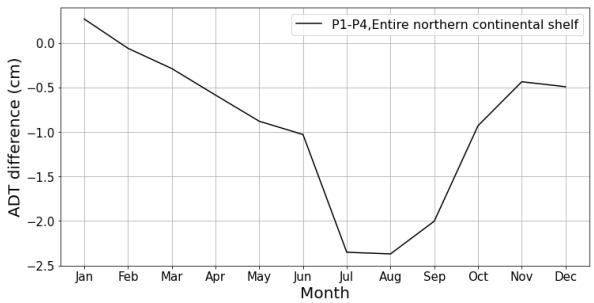

Figure 16. Monthly ADT slopes. a) West bight; b) East bight; c) Entire northern shelf of GoC.

In Figure 15 b) the ADT difference between P3 (CSM) and P4 is shown (Figure 5). Over the entire period positive values are present (P3 > P4). In maximum the ADT at P3 is 2.75 cm higher than at P4 in 2019. In 2006, the ADT at P3 is minimum 0.68 cm higher than at P4. The time series has a positive trend with a yearly increase of 0.02 cm (r-square: 0.13). The monthly ADT difference between P3 and P4 is shown in Figure 16 b). Over the entire year P3 has higher ADT values than P4. Nevertheless, the ADT difference varies over the year. In January the maximum difference of 2.01 cm between P3 and P4 is reached. From January to June the ADT difference is decreasing. In July and August, the ADT difference is first increasing again. Whereupon the difference is decreasing from August again towards October. In October, the lowest ADT difference between P3 and P4 is measured of 0.95 cm. In November and October, the ADT difference is increasing again.

In Figure 15 c) the ADT´s of P1 and P4 are compared (Figure 5). Between 1993 and 1997 the graph shows alternating positive (P1 > P4) and negative (P1 < P4) values. P1 is in maximum 1.18 cm higher than P4 in 1995. From 1998 to 2020, the ADT difference has negative values except for the year 2007. After 2014 to 2020, lower ADT values are present. Further, it is shown that P1 is in maximum -2.26 cm lower than P4 in 2016. The entire time series has a negative trend. A yearly decrease of -0.06 cm (r-square: 0.39) of the ADT difference is observed. Figure 16 c) shows annual ADT difference between P1 and P4. In January the ADT difference has a value of 0.27 which is the only positive value. From February onwards the ADT difference is negative. Furthermore, from February to August the ADT difference is negatively increasing. In maximum P1 is -2.37 cm lower than P4 in August. After August, the ADT difference is decreasing again but stays below zero.

5.2.3 Comparison of slope with velocities

The in-situ measurements of three ADCP`s locations are compared with the ADT slope along the coast. First three time series of the ADCP Quarteira are compared with the ADT slope in the western bight (P1-P2). The two-time series from 2014 and 2015 (not shown) have no significant correlation with the ADT slope. Further, the seasonality and trend of the ADT is removed to check for better correlation. However, this has no influence on the correlation. A significant correlation between the time series of ADCP Quarteira 2020 and the ADT slope is observed (Figure 17 a). The Spearman correlation coefficient is 0.24 (p-value < 0.05). Further a cross correlation is applied. The maximal spearman correlation of 0.33 (p-value < 0.05) is observed with a lag of 2 days. In Figure 17 b) the measurements of the ADCP Armona are compared with the ADT slope of the eastern bight (P3-P4). The time series have a spearman correlation of 0.10 (p-value <0.05). Further, the ADT signal with

removed seasonality and trend is compared with the ADCP signal. Whereby a spearman correlation of 0.12 (p-value <0.05) can be observed. The cross correlation indicates a maximum spearman correlation of 0.13 (p-value <0.05) with a lag of 2 days between the time series. The time series of the ADCP Cacela and the slope (P3-P4) show no significant correlation (not shown).

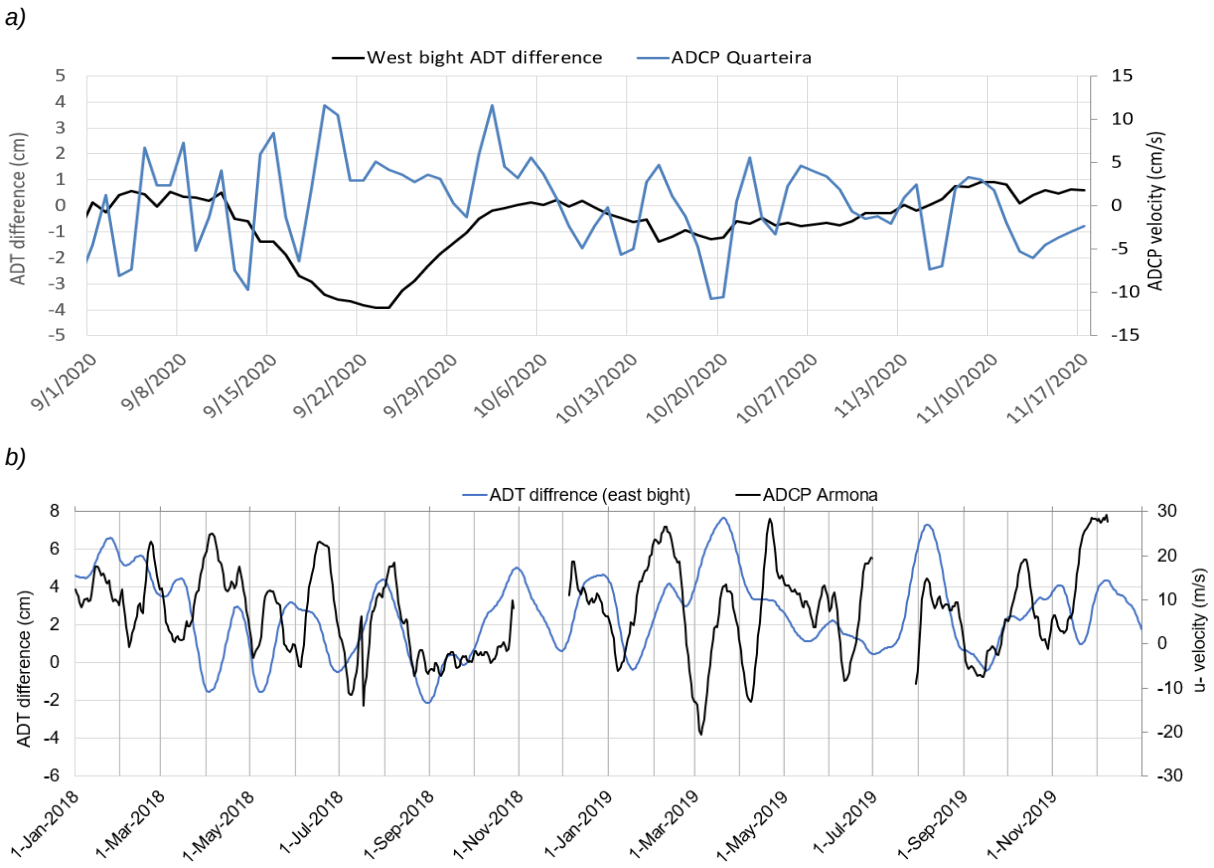

Figure 17. Comparison ADCP and ADT slopes. a) ADCP Quarteira 2020 and ADT difference in the western bight (P1-P2); b) ADCP Armona and ADT difference in the eastern bight (P3-P4).

The time series of the ADT slope is examined for periods of strong negative changes of the ADT differences. These abrupt changes in the ADT indicate an unbalanced slope. In total five time periods are taken in which the ADT changes significantly. These five periods show the largest slope variations of the time series. All slope variations take place between May and October. Four are observed at the west bight (Figure 18 a, b, c, d) and one at the east bight (Figure 18 e) of the GoC. The daily average HFR circulations are visualized at the dates of these initially ADT slope change (red point). Further, the HFR circulations are shown a few days before the actual change (yellow point). These were selected so that they are still in the upward trend before the actual ADT change occurs. The cross correlation between the ADT slope and the ADCPs in the previous chapter suggests that the CCC fully

develop two days after the ADT slope changes. Therefore, the HFR circulations are shown two days after the initial ADT slope change (yellow point). Subsequently the three HFR circulations pictures are compared and examined for flow direction changes. Of the total five unbalanced ADT slope periods, two are described. One in the western bight (18a) and one in the eastern bight (18e) of the GoC. The remaining unbalanced ADT slopes are in the annex. These show similar patterns to the circulations described here.

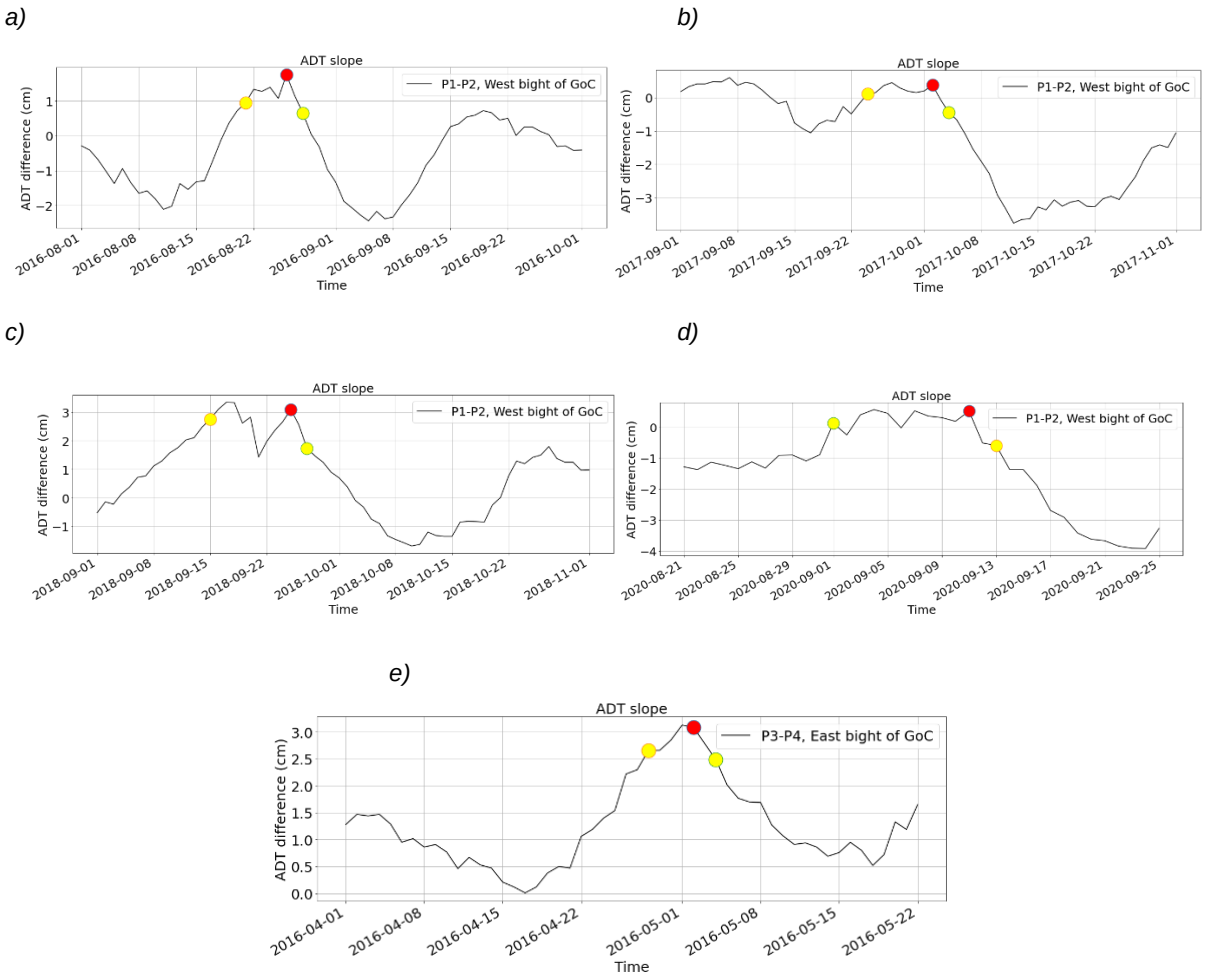

Figure 18. Periods of Unbalanced ADT slopes. a), b), c) and d) unbalanced ADT slope periods at the west bight (P1-P2). e) unbalanced ADT slope periods at the east bight (P3-P4). Red point indicates the initial ADT slope change. Yellow points show the ADT slope few days before and after the ADT slope change.

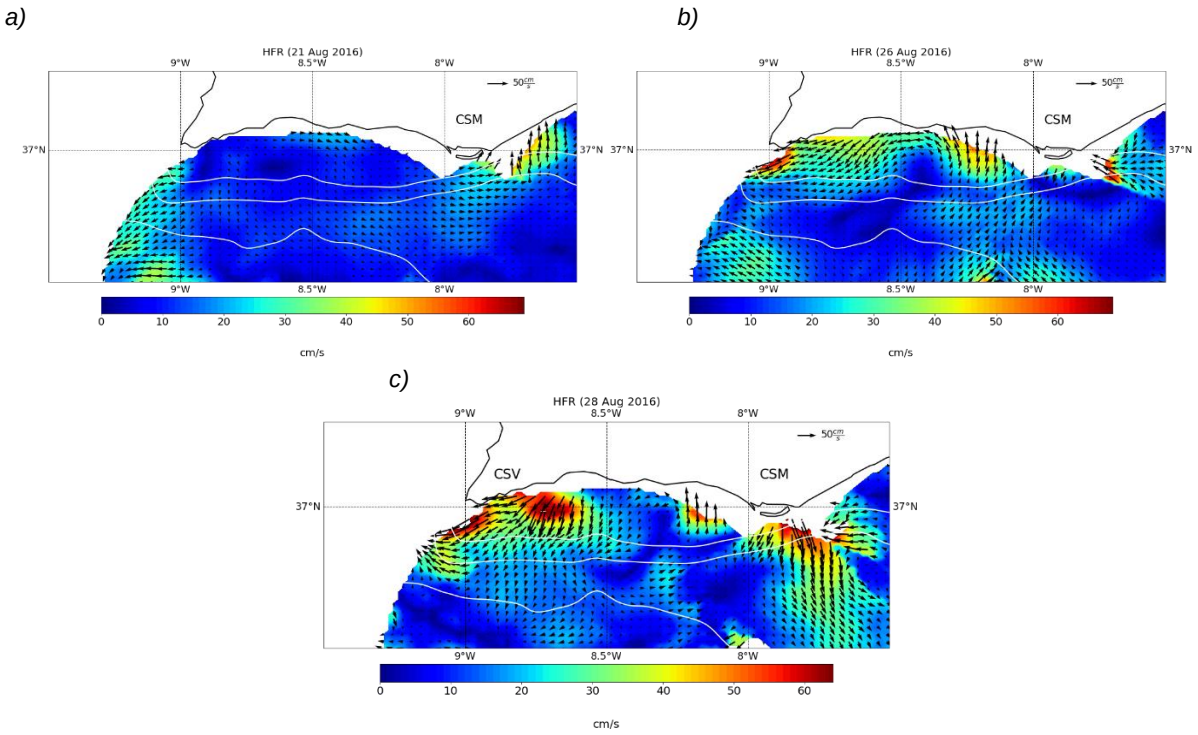

Figure 19. HFR circulations of the GoC west bight (Unbalanced ADT slope: 26 Aug 2016). Isobaths indicate the depths: 250m, 500m 1000m.

Figure 18a shows the ADT slope at the west bight in 2016. The corresponding HRF circulations are presented in Figure 19. At the 21 Aug 2016 the ADT slope had an upward trend (Figure 18a, yellow point at left). The corresponding HRF circulation shows a weak equatorward flow from CSV to CSM (Figure 19a). The 26 Aug 2016 represents the point of the initial change of the ADT slope (Figure 18a, red point). At this date, a current is observed which start flowing northward-west of CSM approximately 30 km offshore which correspond to the depth of 200 m (Figure 19b). The current turns westward as it comes closer to the coast and flows towards CSV. At CSV the flow velocity is increasing. West of CSM a northward flow is visible which starts approximately 25 km offshore. Near the coast from 8° 30'W to 8° 50'W the westward current is weak. However westward from 8° 50'W the current speed increases and is flowing to the south-west. Further, the 28 Aug 2016 (Figure 18a, yellow point at right) is taken which is two days after the initial change. In general, it is observed that the CCC on the 28 Aug 2016 (Figure 19c) were higher compared to the date of the initial ADT slope change especially around CSM and CSV.

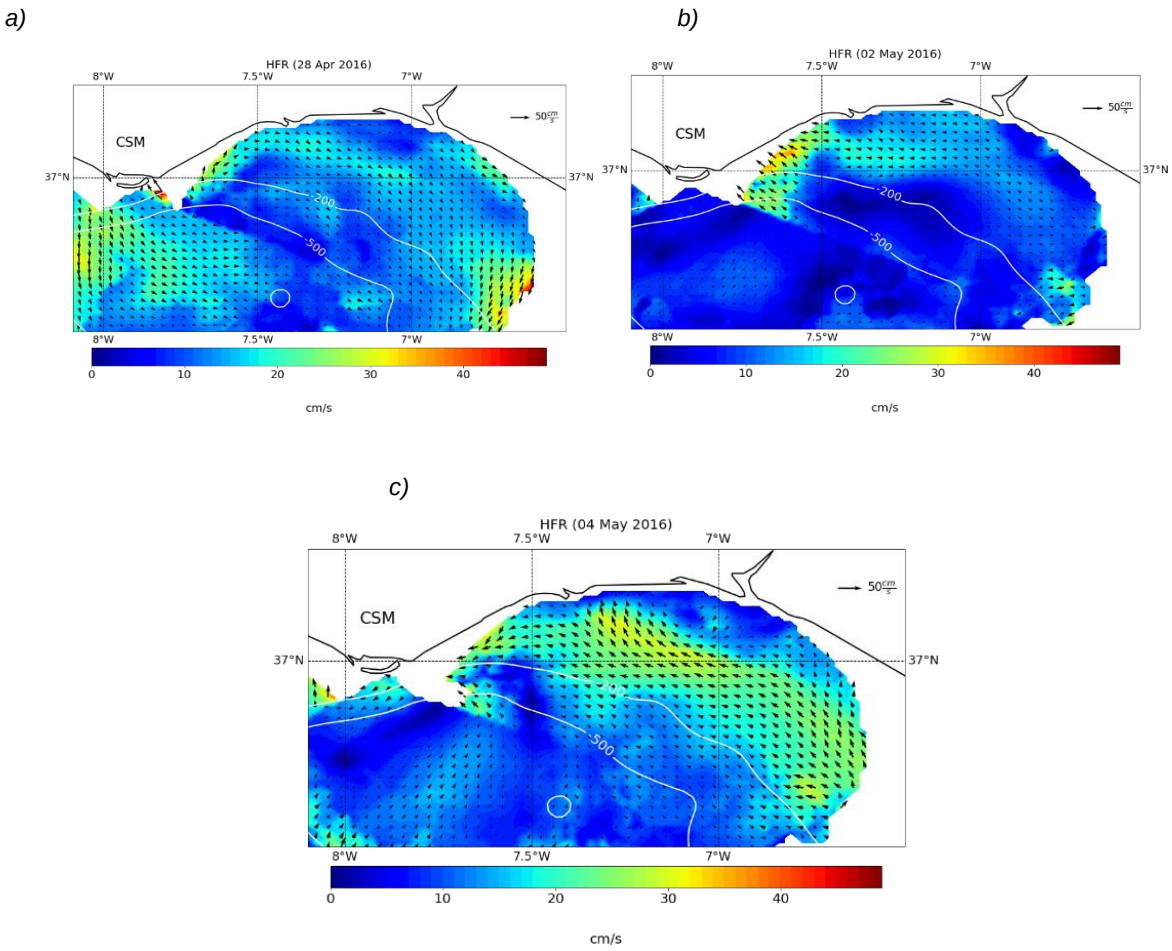

Figure 20. HFR circulations of the GoC east bight (Unbalanced ADT slope: 04 May 2016)

Figure 18e represents the ADT slope of the eastern bight of the GoC in 2016. Figure 20a shows the HFR circulations on the 28 Apr 2016, four days before the ADT change. East of CSM an equatorward flow is visible which follows roughly the coast of the eastern bight of the GoC. However, no CCC was detected on the 28 Apr 2020. The initial change of the ADT slope occurred on the 02 May 2016 (Figure 20 b). West of 7° W a weak westward flowing current is visible which is not flowing beyond the 200 m bathymetry contour. The current increases towards CSM and changes the direction to north-west. Further, near CSM the current is observed beyond the 500 m bathymetry. Figure 20c shows the HFR circulations on the 04 May 2016, two days after the initial change of the ADT slope is displayed. Within the 200 m bathymetry contour a north-westward flowing current is visible. The currents on the 04 May 2016 were stronger than these on the 02 May 2016.

6. Discussion

6.1 Characterization of the ADT and geostrophic circulations of the entire GoC

The first part of this work has focused on the characterization of the ADT and geostrophic current of the entire GoC. The average linear ADT trend of 3.15 mm/year (R^2: 0.85) is in good agreement with other studies (Vargas-Yáñez et al., 2021). In the 28 years, the average ADT increased 8.82 cm in the GoC. The ADT increase is significantly larger (8.82 cm) than the average ADT error of 2 cm. Vargas-Yáñez et al. (2021) show that the sea level in the GoC rose between 1.5 – 4.6 mm/year between 1990 and 2018. Further, the linear ADT increase is in good agreement with the global sea level rise of 3.1+/- 0.3 mm/year obtained from satellite altimetry data between 1993 and 2018 (Cazenave et al., 2018). The global sea level rise is affecting the GoC and can be detected with satellite altimetry data. Moreover, the average ADT signal reveals that the GoC has an unequal ADT pattern. In general, it is observed that the ADT rises from north to south. The Spearman correlation between the average ADT and SST shows that the ADT variation is partly due to the effect of thermal expansion of water. The magnitude of the correlation coefficient of 0.29 to 0.62 (p-value < 0.05) indicates that the effect of thermal expansion plays a key role for the variation of sea level. Indeed, previous studies suggest that sea level variation is mainly driven by the effect of thermal expansion (Garcia-Lafuente at al. 2004, 2007; Gómez-Enri et al. 2011; Laiz et al. 2012; Vargas-Yáñez et al., 2021). It could be shown that the maximum of the ADT has a lag of two months behind the SST. However, over the shelf area of the GoC, the ADT/SST shows mostly a low correlation (< 0.5). This can be attributed to the fact that other effects have a greater influence in the shelf area e.g., river discharge, low atmospheric pressure or storm surges (Garcia-Lafuente at al. 2004, 2007; Gómez-Enri et al. 2011).

The seasonal analysis shows that the ADT pattern varies over the annual cycle. The highest seasonal ADT is reached in autumn and the lowest seasonal ADT in spring. This observation agrees with the study of Garcia-Lafuente at al. (2007), which detected the maximum and minimum sea level in September and March, respectively, through altimetry data analysis from 1992 - 2005. The seasonal ADT anomaly maps revealed controversial patterns. In winter, the interior of the GoC indicate lower ADT anomaly values whereby the shelf area has higher ADT anomaly values. In summer, it is the opposite. The interior of the GoC shows higher values and the shelf mostly lower values. By studying the geostrophic circulation, it is shown that they have a similar pattern as the ADTs. The geostrophic current anomaly map indicates that the equatorward current over the shelf is stronger in summer. This can be explained by strong northerly winds in summer, which form equatorward propagating upwelling fronts (Relvas, Barton, 2002, 2005; Sanchez and Relvas 2003;

Vargas et al. 2003). The upwelling fronts transport cold water along the shelf, which can explain the low ADT anomaly values due to thermal expansion over the entire shelf of the study area. The interior of the GoC mostly shows lower geostrophic velocities in summer. Klein and Siedler (1989) show that the Azores Current moves southward during summer and has as such a lower influence on the GoC circulations than in winter. Thus, the speed of the currents inside the GoC are weaker in summer (Carracedoa et al. 2014; Johnson and Stevens 1999; Klein and Siedler, 1989; Martins et al., 2002). In winter, however the shelf circulation is weaker due to the absence of strong favorable upwelling winds (Relvas, Barton, 2002, 2005; Sanchez and Relvas 2003; Vargas et al. 2003). Subsequently, the ADT is higher due to the absence of cold upwelling fronts. However, in winter the Azores Current reaches the GoC whereby the stronger currents in the interior of the GoC can be explained (Carracedoa et al. 2014; Johnson and Stevens 1999; Klein and Siedler, 1989; Martins et al., 2002).

Further, it is shown that the seasonal circulation pattern has an influence on the origin of the inflowing water of the SG. In summer, the inflowing water of the SG originates from the northern shelf of the GoC. Whereby during winter, the inflowing water comes more from the interior of the GoC. This observation is consistent with SST study by Folkard et al. (1997) and the numerical model by Jia (2000). Folkard et al. (1997) assumed that in summer an eastward extension of upwelled water flows over the northern shelf of the GoC and enters the SG. Jia (2000) suggests that the seasonal meridional shift of the Azores Current is mainly responsible of the origin of the inflowing water into the SG.

6.2 Characterization of the northern continental shelf of the GoC

In the second part of this thesis, the potential effects of water level variations on circulation patterns at the northern shelf of the Gulf of Cadiz were explored. The velocity measurements of the ADCP`s Quarteira, Armona and Cacela were compared with the respective grid point of the geostrophic flow. The investigation showed that no or very weak correlation could be found. The ADCP devices are deployed at depths from 9 m to 23 m. In this shallow water depth, bottom friction plays a crucial role, which is neglected by the calculation of the geostrophic current. Hence, it was shown that the shelf circulation is mostly non-geostrophic as expected.

Further, special attention has been devoted to the correlation between the development of westward flows (CCC) along the coast and variations in the alongshore slope. It is assumed that CCC develops due to unbalance alongshore pressure gradient (De Oliveira Junior et al., 2021; De Oliveira Junior et al., 2022; Garel et al. 2016). HFR data have been used to detect

CCC. Alongshore pressure gradients were revealed by the calculation of the ADT slope. To validate the ADT records near the coast, they have been compared with in situ measurements of two Tidal gauge stations. This method is a suitable way to validate the ADT near the coast (Gómez-Enri et al. 2011; Lin et al. 2021; Saraceno et al., 2008). The analysis shows that the measurements of the tidal gauge station Huelva and the respective ADT has a Spearman's correlation coefficient of 0.52 (p-value < 0.05). The Bonanza station measurements and the respective ADT has a Spearman's correlation coefficient of 0.51 (p-value < 0.05). This corresponds to a moderate correlation. This can be attributed to the higher ADT error above the shelf area, which can result in a lower correlation (Copernicus, 2022; Mulet et al., 2021; Rio et al.,2011). Gómez-Enri et al. (2019) determined great uncertainties of the MDT over the shelf area of the GoC. Considering the construction of the ADT, the MDT error is also present in ADT. For further studies of the alongshore slope it is therefore recommended to use SLA instead of ADT. However, by consideration of the distance of the ADT grid point and the Tidal gauge station of approximately 12 km to 20 km and the spatial resolution of 0,125° x 0,125° this can be considered as a good correspondence. However, Gómez-Enri et al. (2011) showed that the goodness of fit between tidal gauge and gridded altimetry data was increased from 39.5% to 88.2% by correction of atmospheric pressure and the river discharge effects in the GoC. It is recommended that future ADT alongshore slopes studies take these effects into account.

ADT alongshore slopes are revealed at the western bight, eastern bight and over the entire northern shelf of the GoC. The ADT slopes indicate trends between -0.06 cm/year and 0.02 cm/year. However, all trends have very low r-square values (<0.4). These results must be considered with caution as the ADT slope magnitudes are within the ADT error margin of 2 cm. Nevertheless, correspondences of the ADT slope with costal alongshore HFR flows can be observed. The ADT slopes, in the west and east bight of the GoC are sloping mainly towards the east. This is consistent with a predominantly anticyclonic circulation in the GoC (Criado-Aldeanueva et al. 2006, 2009; De Oliveira Junior et al., 2022; Lafuente and Ruiz, 2007; Vargas et al. 2003). Moreover, the monthly ADT slope at the western bight indicates an ADT sloping towards the east except for the month June, September, and August. In these summer months the slope is the opposite. This observation corresponds with the period of upwelling events due to strong winds (Fuiza et al., 1981; Relvas and Barton, 2004). The upwelling events during the summer season could be responsible for colder water and therefore lower ADTs at the west coast of Portugal which results in a reversal of the slope. Moreover, the monthly ADT slope over the entire northern shelf of the GoC (P1-P4) shows a similar seasonal pattern.

The ADT slope and the ADCP measurements have no or low Spearman correlation (< 0.25). However, the best correlation was obtained by cross correlation (< 0.34) where the ADCP speed has a lag of 2 days to the ADT slope. The low correlation shows that the slope dose not always correspond to the current variations in direction. Instead, previous studies suggest that the ADT along shore slope is the driver of CCC just at very specific moments, when the alongshore pressure gradient gets unbalanced (De Oliveira Junior et al., 2021; De Oliveira Junior et al., 2022; Garel et al. 2016). Five ADT slope periods are selected where the along shore pressure gradient gets unbalanced. HFR circulation data is used to detect CCC during these periods. The HFR plots show that CCC develops during all five periods. It is observed that it is irrelevant in which direction the ADT slope is sloping when the CCC start to develop. However, crucial is that the ADT slope time series experience a strong negative change which indicates an unbalanced ADT slope. These observations are in good agreement with the previous studies (De Oliveira Junior et al., 2021; De Oliveira Junior et al., 2022; Garel et al. 2016). Furthermore, it could be shown that the CCC became stronger two days after the initial ADT change.

7. Conclusion

In this thesis, satellite altimetry data from 28 years were used to characterize the sea level and geostrophic circulation patterns in the GoC. The ADT analysis could show that the GoC is influenced by the sea level rise and its trend is in good agreement with the global trend. The effect of thermal expansion plays a key role in the variation of sea level.

The analysis of the ADT and geostrophic current patterns revealed two seasonal circulation modes. In summer, strong equatorward currents occur along the shelf slope, whereas the currents in the interior of the GoC are weaker. However, in winter the opposite occurs. The currents are stronger in the interior of the GoC and weaker over the shelf area. Two mechanisms could be identified for these countervailing patterns. The occurrence of strong northerly winds which form upwelling fronts over the shelf in summer and the Azores Current which reaches the GoC in winter.

Furthermore, the potential effects of water level variations on circulation patterns at the northern shelf of the GoC were explored. ADCP measurements have shown that the shelf circulations are mainly non-geostrophic. Although the ADT over the shelf area has large uncertainties, moderate to good correlations between tidal gauge stations and ADT could be determined. Moreover, ADT measurements were suitable to identify unbalanced alongshore pressure gradients. However, for further studies of the alongshore slope it is recommended

to use SLA instead of ADT due to smaller uncertainties. By using HFR circulation data it was shown that CCC development corresponds to the unbalance along-shore pressure gradients. Furthermore, the HFR circulations data demonstrated that CCC reached their maximum two days after the slope became unbalanced.

8. References

Ambara, I., Serraa, N., Brogueirab, M. J., Cabe-cadasb, G., Abrantesc, F., Freitasc, P., Goncalvesb, C., Gonzalez, N. (2000). Physical, chemical and sedimentological aspects of the Mediterranean outflow off Iberia. Deep-Sea Research II 49, 4163–4177.

Autret, E., Tandeo, P., Paul, F.,. (2021). CMEMS Product User Manual for the L4 reprocessed ODYSSEA product over the European North West Shelves. EU Copernicus Marine service.

Carracedo, L. I., Gilcoto M., Mercier, H., Pérez, F. F. (2014). Seasonal dynamics in the Azores–Gibraltar Strait region: A climatologically-based study. Progress in Oceanography 122, 116–130.

Copernicus, (2022). Marine Copernicus. https://www.copernicus.eu/en/copernicus-services/marine. Copernicus Marine Service, Ocean Products.

https://resources.marine.copernicus.eu/products

Criado-Aldeanueva, F., Del Río Vera, V., García-Lafuente, J. (2007). Steric and mass-induced Mediterranean sea level trends from 14 years of altimetry data. Global and Planetary Change 60, 563–575.

Criado-Aldeanueva, F., Garcia-Lafuente, J., Navarro, G., Ruiz, J.,. (2009). Seasonal and interannual variability of the surface circulation in the eastern Gulf of Cadiz (SW Iberia). Journal of geophysical research 114.

Criado-Aldeanueva, F., Garcia-Lafuente, J., Vargas, J.M, Del Rio, J., Vazquez, A., Reul, A., Sanchez, A.,. (2006). Distribution and circulation of water masses in the Gulf of Cadiz from in situ observations. Deep-Sea Research II 53, 1144–1160.

De Oliveira Júnior, L., Garel, E., Relvas, P. . (2021). The structure of incipient coastal counter currents in South Portugal as indicator of their forcing agents. Journal of Marine Systems.

De Oliveira Júnior, L., Relvas, P., Garel, E. (2022). Kinematics of surface currents at the northern margin. European Geosciences Union, Ocean Science 18, 1183–1202.

Fiuza, A. F., Macedo, M. E., Guerreiro, M. R. (1981). Climatological space and time variation of the Portuguese coastal upwelling. Oceanologica Acta 1982, Vol. 5, Nr. 1.

Folkard, A. M., Davies, A., Fiuza, A. F. G., Ambar, I. (1997). Remotely sensed sea surface thermal patterns in the Gulf of Cadiz and the Strait of Gibraltar: Variability, correlations, and relationships with the surface wind field. Journal of geophysical research 102, 5669-5683.

Garcia Lafuente, J., Ruiz, J. (2007). The Gulf of Cadiz pelagic ecosystem: A review. Progress in Oceanography 74, 228–251.

Garcia-Lafuent, J., Delgad, J., Criado-Aldeanueva, F., Bruno, M., Del Rio, J., Vargas, J.M. (2006). Water mass circulation on the continental shelf of the Gulf of Cadiz. Deep-Sea Research II 53, 1182–1197.

Garcia-Lafuente, J., Del Rio, J., Alvarez Fanjul, E., Gomis, D., Delgado., J. (2004). Some aspects of the seasonal sea level variations around Spain. JOURNAL OF GEOPHYSICAL RESEARCH, VOL. 109.

Garel, E., Drago, T., Relvas, P. (2016). Characterisation of coastal counter-currents on the inner shelf of the Gulf of Cadiz. Journal of Marine Systems 155, 19-34.

Gómez-Enri, ., Aboitiz, A.Tejedor, B., Villares, P. (2011). Seasonal and interannual variability in the Gulf of Cadiz: Validation of gridded altimeter products. Estuarine, Coastal and Shelf Science 96, 114-121.

Gómez-Enria, J., Gonzáleza, C. J., Passarob, M., Vignudellic, S., Álvareza, O., Cipollinid, P., Mañanesa, R., Brunoa, M., López-Carmonae, M. P., Izquierdoa, A. (2019). Wind-induced cross-strait sea level variability in the Strait of Gibraltar from coastal altimetry and in-situ measurements. Remote Sensing of Environment 221, 596–608.

Jia, Y. (1999). Formation of an Azores Current Due to Mediterranean Overflow in a Modeling Study of the North Atlantic. Journal of physical oceanography 30.

Johnson, J., Stevens, I. (1999). A "ne resolution model of the eastern North Atlantic between the Azores, the Canary Islands and the Gibraltar Strait. Deep-Sea Research I 47, 875-899.

Kida, S. (2006). Overflows and Upper Ocean Interaction: A Mechanism for the Azores Current. Woods Hole Oceanographic Institution MA.

Klein, B., Siedler, G. (1989). On the Origin of the Azores Current. Journal of Geophysical research, Vol. 94,, 6159-6168,.

Lago,L. S., Saraceno, M., Piola, A. R., Ruiz-Etcheverry, L. A. (2021). Volume Transport Variability on the Northern Argentine Continental Shelf From In Situ and Satellite Altimetry Data. Journal of Geophysical Research: Oceans, 126.

Laiz, I., Gomez-Enri, J., Tejedor, B., Aboitiz, A., Villares, P. (2012). Seasonal sea level variations in the gulf of Cadiz continental shelf from in-situ measurements and satellite altimetry. Continental Shel fResearch, 53, 77–88.

Laiz, I., Plecha, S., Teles-Machado, A., González-Ortegón, E., Sánchez-Quiles, D., Cobelo-García, A., Roque, D., Peliz, A., Sánchez-Leal, R. F. Tovar-Sánchez, A. (2019). The role of the Gulf of Cadiz circulation in the redistribution of trace metals between the Atlantic Ocean and the Mediterranean Sea. Science of the Total Environment 719.

Lin, W., Lin, H., Hu, J. (2021). The Tilt of Mean Dynamic Topography and its Seasonality Along the Coast of the Chinese Mainland. Journal of Geophysical Research: Oceans, 126.

Machin, F., Pelegri, J.L., Marrero-Diaz, A.,Laiz, I., Ratsimandresy A.W. (2006). Near-surface circulation in the southern Gulf of Cadiz. Deep-Sea Research II 53, 1161–1181.

Mason, E., Colas, F., Molemaker, J., Shchepetkin, A. F. (2011). Seasonal variability of the Canary Current: A numerical study. JOURNAL OF GEOPHYSICAL RESEARCH, VOL. 116,.

Mulet, S., Rio, M.H., Etienne, H., Artana, C., Cancet, M., Dibarboure, G., Feng, H., Husson, R., Picot, N., Provost, C., Strub, P.T,. (2021). The new CNES-CLS18 global mean dynamic topography. Ocean Science 17, 789-808.

Peliz, A., Boutov, D., Cardoso, R. M., Delgado, J., Soares, P.,. (2013). The Gulf of Cadiz–Alboran Sea sub-basin: Model setup, exchange and seasonal variability. Ocean Modelling 61, 49–67.

Peliz, A., Dubert, J., Marchesiello, P., Teles-Machado, A. (2007). Surface circulation in the Gulf of Cadiz: Model and mean flow structure Model and mean flow structure. Journal of geophysical research 112.

Peliz, A., Marchesiello, P., Santos, A. M., Dubert, J., Teles-Machado, A., Marta-Almeida, M., Le Cann, B. (2009). Surface circulation in the Gulf of Cadiz: 2. Inflow-outflow coupling and the Gulf of Cadiz slope current. Journal of geophysical research 114.

Perez, F.F., Castro, C.G., Alvarez-Salgado, X.A., Riuos, A.F.,. (2001). Coupling between the Iberian basin-scale circulation and the Portugal boundary current system: a chemical study. Deep-Sea Research I 48, 1519 -1533.

Pujol, M. I., Faugère, Y., Taburet, G., Dupuy, S., Pelloquin, C., Ablain, M., Picot, N. (2016). DUACS DT2014: the new multi-mission altimeter data set reprocessed over 20 years. European Geosciences Union (EGU): Ocean Science 12, 1067–1090.

Relvas, P., Barton, E. D. (2002). Mesoscale patterns in the Cape Sao Vicente (Iberian Peninsula) upwelling region. ournal of geophysical research 107.

Relvas, P., Barton, E.D.,. (2005). A separated jet and coastal counterflow during upwelling relaxation off Cape Sao Vicente (Iberian Peninsula). Continental Shelf Research 25, 29–49.

CEMES, (2017). Report on European HF Radar systems development and roadmap for HF Radar products evolution in compliance with CMEMS needs. European HF Radar systems development and roadmap for HF Radar in CMEMS.

Rio, M. H., Guinehut, S., Larnicol, G. (2011). New CNES-CLS09 global mean dynamic topography computed from the combination of GRACE data, altimetry, and in situ measurements. JOURNAL OF GEOPHYSICAL RESEARCH, VOL. 116.

Ruiz Etcheverry, L. A., Saraceno, M., Piola A. R., Strub, P. T. (2016). Sea level anomaly on the Patagonian continental shelf: Trends, annual patterns and geostrophic flows. Journal of Geophysical Research: Oceans, 121, 2733–2754,.

Sanchez, R. F., Mason, E., Relvas, P., Da Silva, A. J., Peliz, A. . (2006). On the inner-shelf circulation in the northern Gulf of Cadiz, southern Portuguese shelf. Deep-Sea Research II 53, 1198–1218.

Sanchez, R. F., Relvas, P. . (2003). Spring–summer climatological circulation in the upper layer in the region of Cape St. Vincent, Southwest Portugal. ICES Journal of Marine Science 60, 232–1250.

Saraceno, M., Strub, P. T., Kosro. P.M. (2008). Estimates of sea surface height and near-surface alongshore coastal currents from combinations of altimeters and tide gauges. Journal of Geophysical research, Vol. 113.

Sena Martins, C.., Hamann, M., Fiuza, A. F. G. (2002). Surface circulation in the eastern North Atlantic, from drifters and altimetry. Journal of Geophysical research, Vol. 107.

Soto-Navarro, J., Criado-Aldeanueva, F., García-Lafuente, J., Sánchez-Román, A. (2010). Estimation of the Atlantic inflow through the Strait of Gibraltar from climatological and in situ data. Journal of Geophysical research, Vol. 115,.

Swart, N. S. (2010). Schematic of geostrophic flow.

Vargas, J.M., Garcia-Lafuente, J., Delgado, J., Criado, F. (2003). Seasonal and wind-induced variability of Sea Surface Temperature patterns in the Gulf of Cadiz. Journal of Marine Systems 38, 205-219.

Vargas-Yáñez, M., Tel, E., Moya, F., Ballesteros, E., García-Martínez, M. C. (2021). Long-Term Changes, Inter-Annual, and Monthly Variability of Sea Level at the Coasts of the Spanish Mediterranean and the Gulf of Cádiz. Geosciences 2021, 11, 350.

WCRP Global Sea Level Budget Group, C. C. (2018). Global sea-level budget 1993–present. Earth System Science Data, 10, 1551–1590.

9. Annex

SLA error

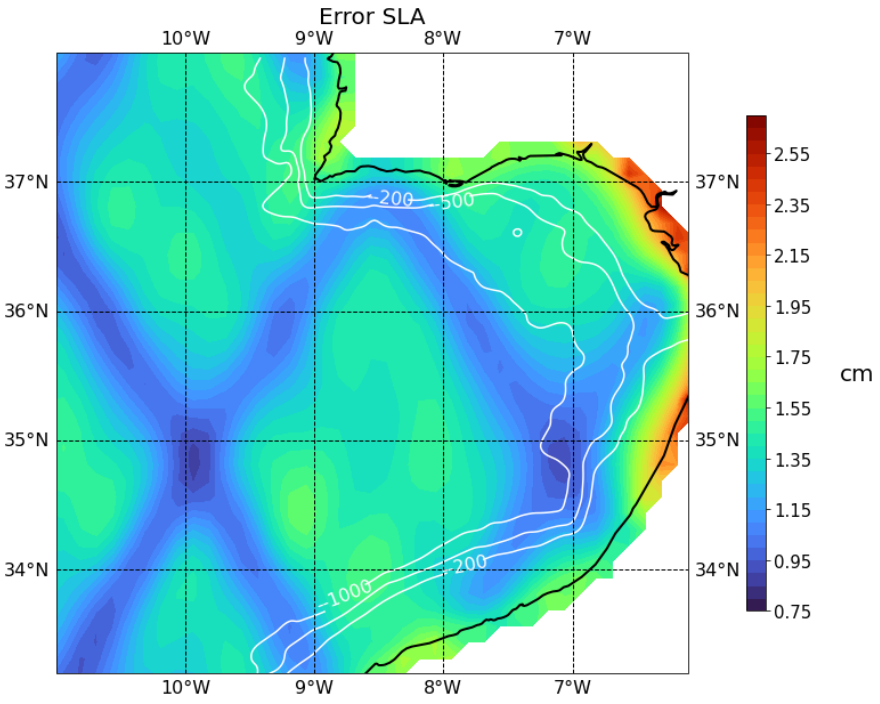

Mean SLA error

Seasonal ADT

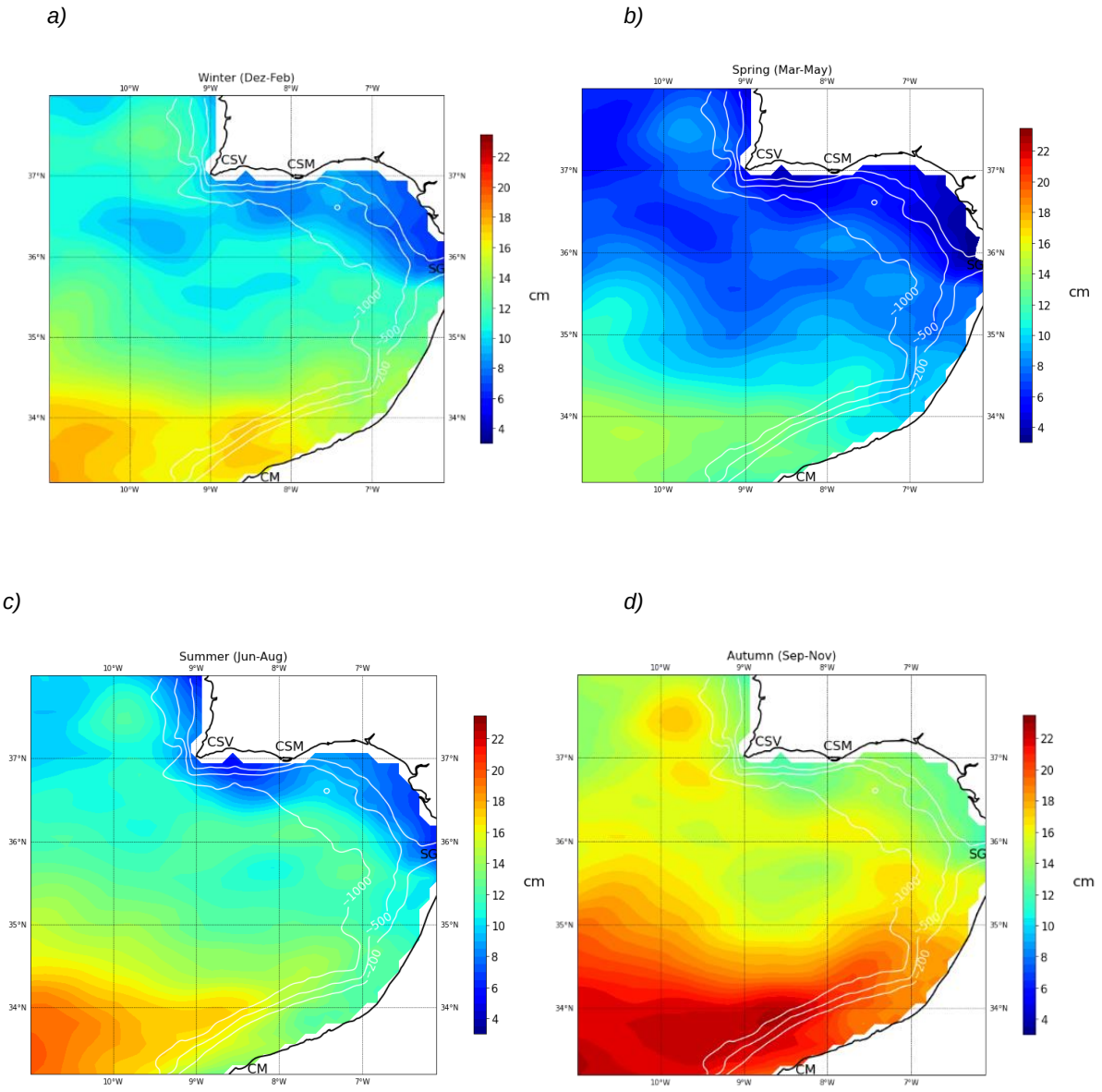

Seasonal ADT. a) Winter, b) Spring, c) Summer, d) Autumn.

Seasonal geostrophic current

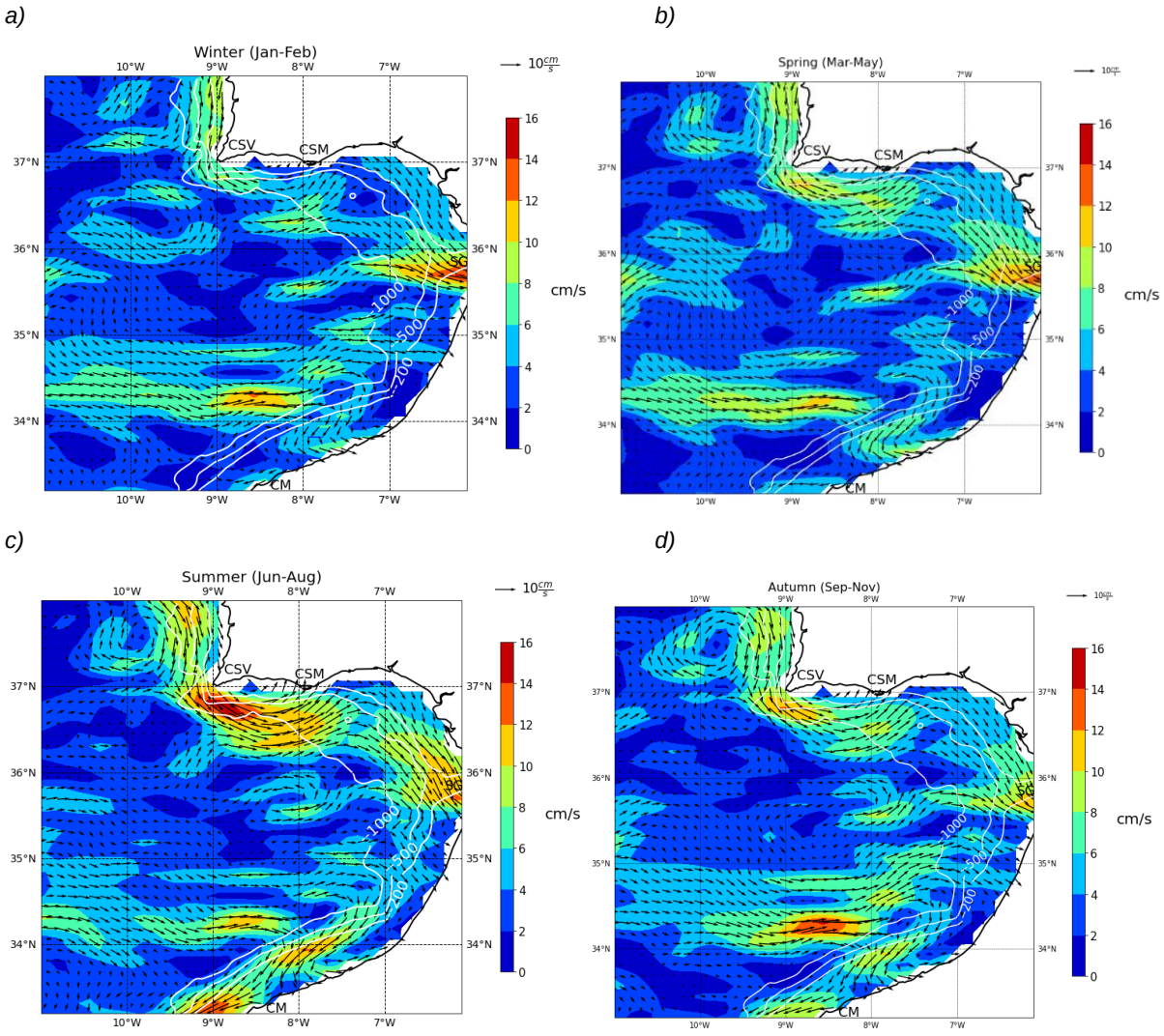

Seasonal surface geostrophic current patterns. For each season, the average geostrophic flows and the seasonal anomaly are shown. a), b) Winter; c), d) Summer.

Tidal gauge trend

a)

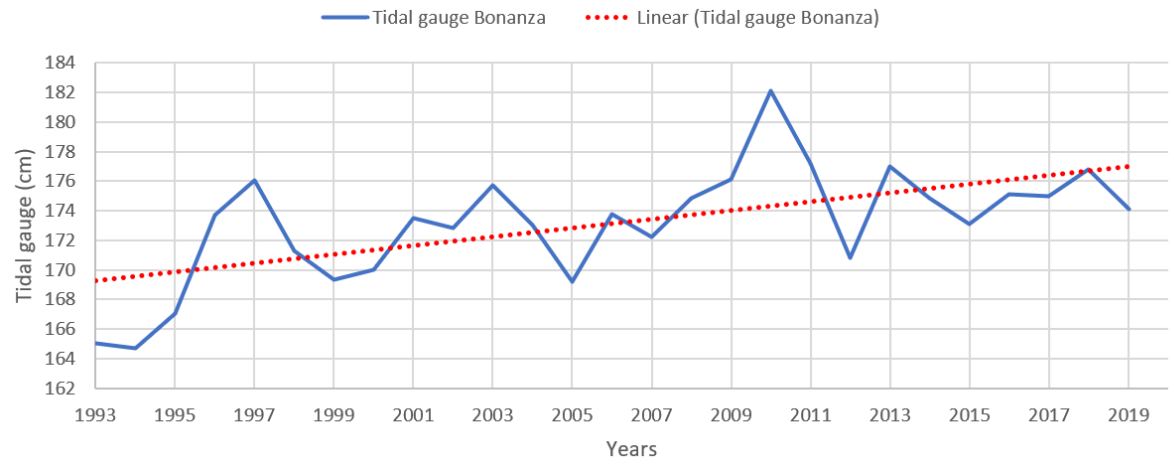

b)

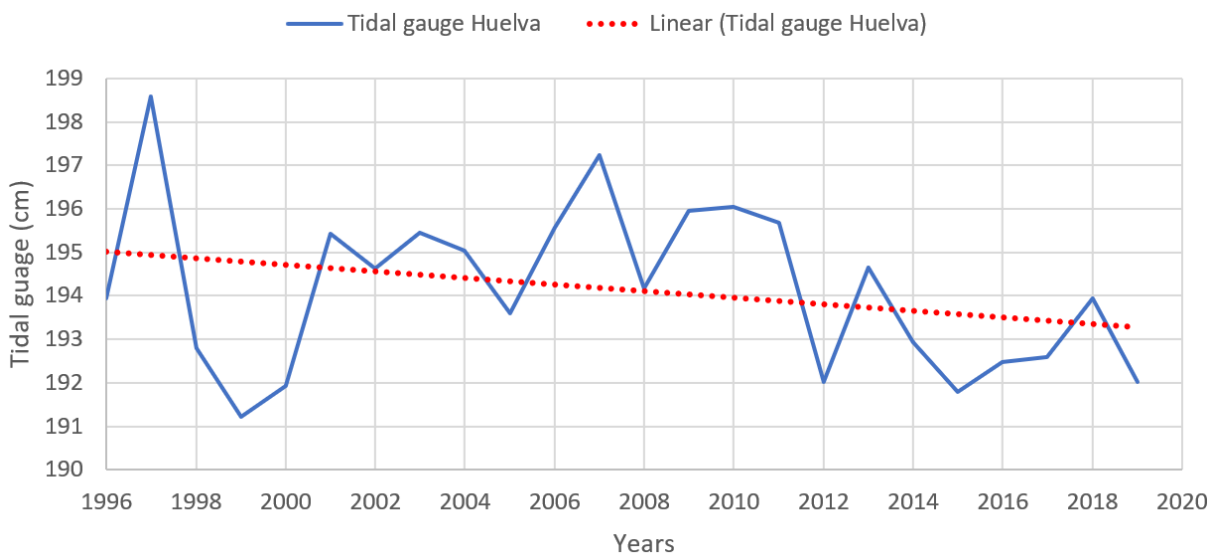

Tidal gauge measurements with trend line. a) Bonanza; b) Huelva.

HFR circulations

The HFR circulations on the 23 Sep 2017 are shown, few days before the initial ADT slope change. In the western bight of the GoC the flow is predominantly south-west. West of CSM the flow increases in speed and is heading south. In total no CCC are observed on the 23 Sep 2017. On the initial date (02 Oct 2017) of change it is observed that the counter current start to develop near the coast westward of 8° 30'W. The flow has predominantly a south-westward direction. Further the current increases at the CSV and also flows south westward over the 1000 m bathymetry contour into the GoC. The HFR circulations of the 04 Oct 2017 are shown. The circulations have a similar pattern than two days before. However, it can be clearly seen that the current speed has increased.

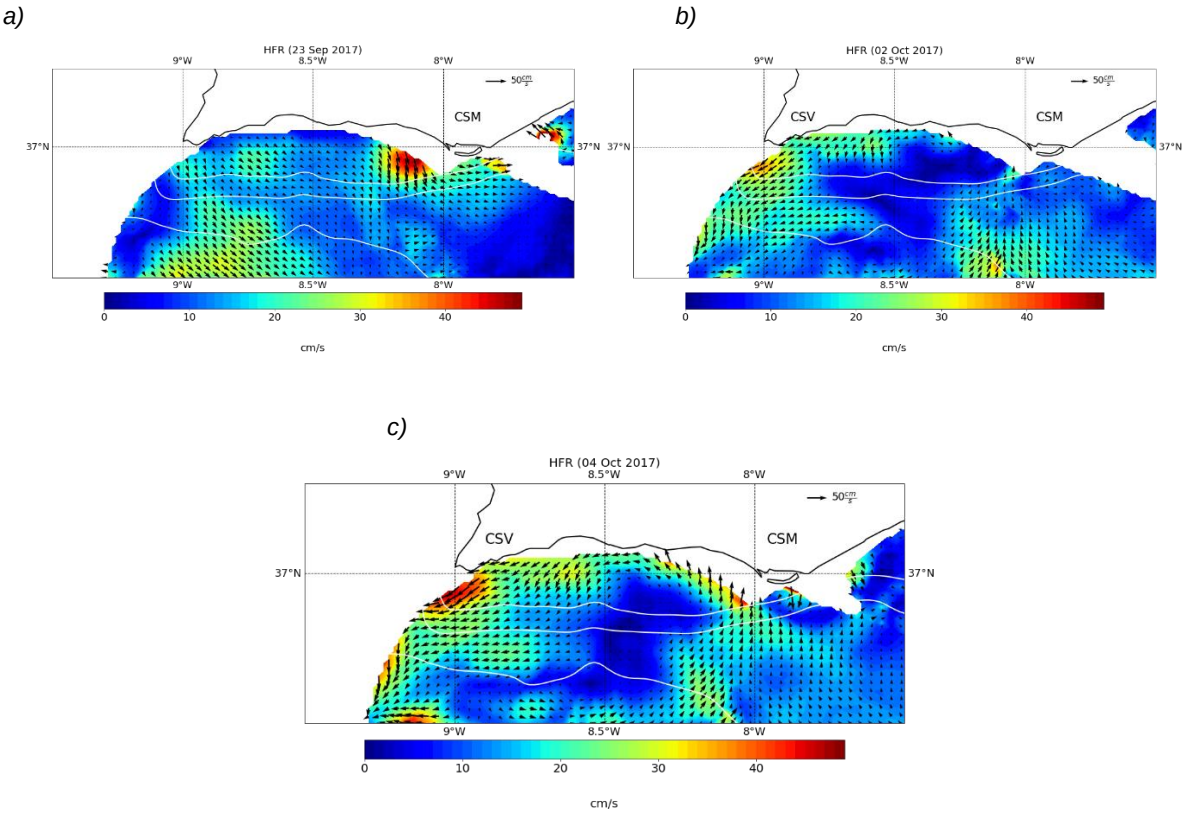

HFR circulations of the GoC west bight (Unbalanced ADT slope: 04 Oct 2017)

At the 15 Sep 2018 the ADT slope has an upward trend. However, the related HFR circulations show a weak but poleward flow along the western bight of the GoC. Near CSV the flow turns to the south-west and increase in speed. The initial date of the ADT change is 25 Sep 2018. Westward of CSM a northward flow can be observed which changes direction to west. The current propagates over the shelf to CSV. South of CSV the current increases in speed. However, the flow doesn't continue over the 200 m bathymetry contour. Further the two days delayed HFR circulations (27 Sep 2018) are visualized. It is observed that the counter current develops west of CSM. As the current penetrates to the west it changes direction from north-west to west to south-west near CSV. Further, at CSV the current is increasing. The flow doesn't flow beyond the 200 m bathymetry contour. In general, the flow at the 27 Sep 2018 is stronger than two days before on the 25 Sep 2018.

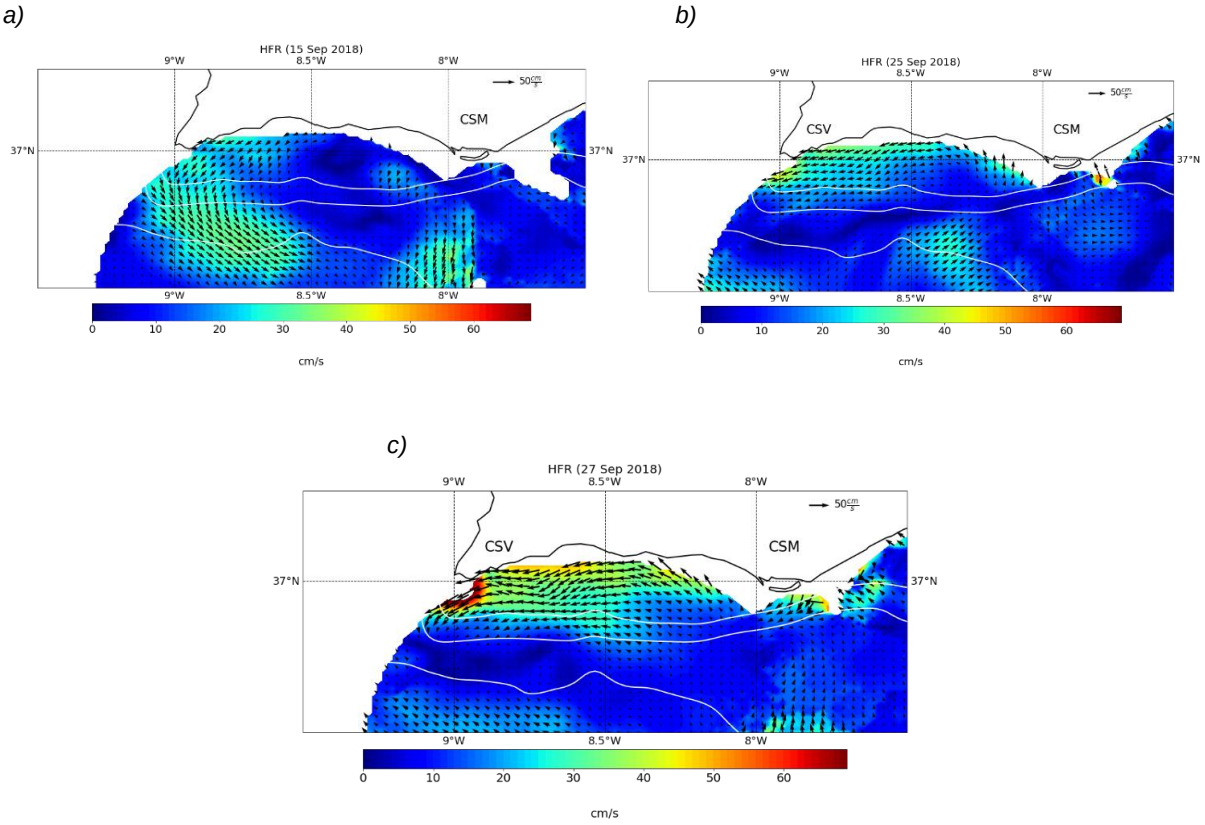

HFR circulations of the GoC west bight (Unbalanced ADT slope: 27 Sep 2018)

At the 01 Sep 2020 the, few days before the initial ADT change no CCC are observed. The flow is predominantly west to south-west. The ADT slope changes on the 11 Sep 2020. West of CSM approximately 25 km offshore a northward flowing current develops. Westward of 8° 50'W a current is observed which flows in west to south-west direction. The HFR circulation two days after the initial ADT slope change (13 Sep 2020) is visualized. West of CSM a flow is observed which develops approximately 35 km offshore which corresponds to a depth of 500 m. The flow magnitude increases close to the shore. From there the current flows to the west were it first decreases and than again increases towards CSV. As the current reach CSV, it changes direction from west to south-west. Further the current flows beyond the 1000 m bathymetry into the GoC. The CCC on the 13 Sep 2020 are stronger than on the date of the initial ADT slope change.

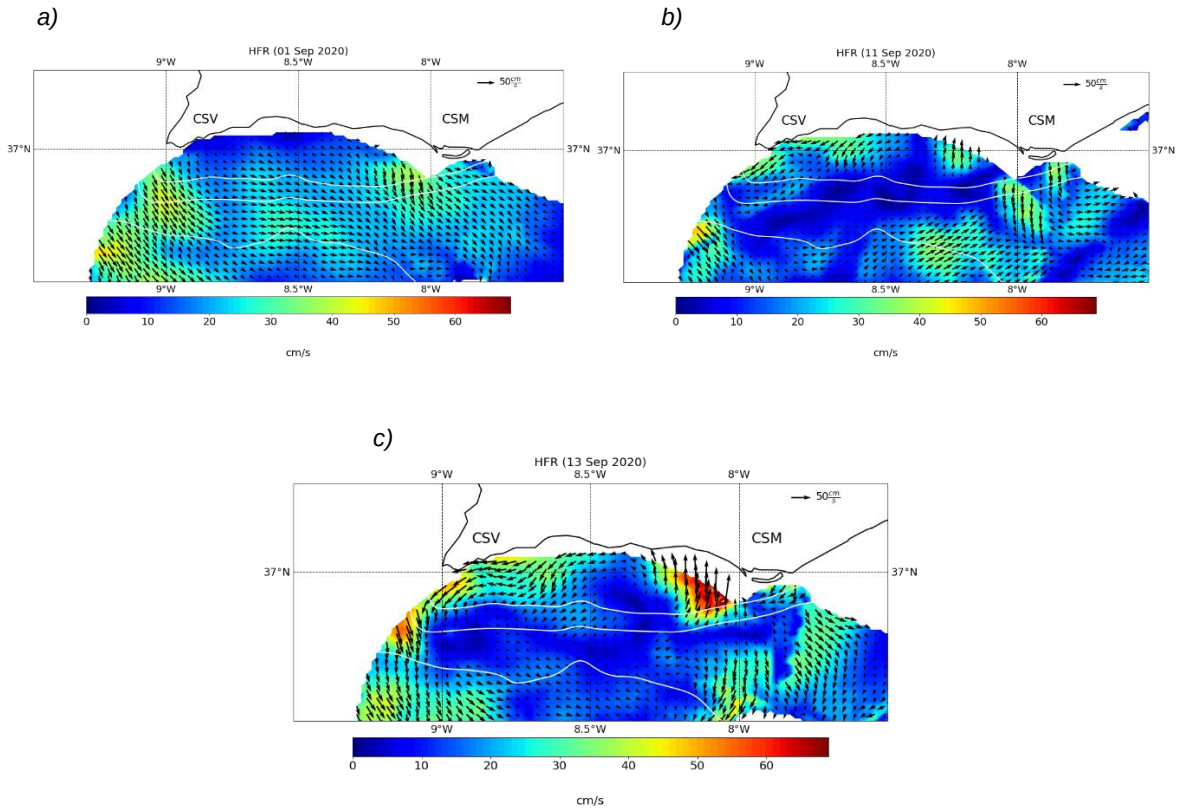

HFR circulations of the GoC west bight (Unbalanced ADT slope: 11 Sep 2020)